TTG and potassic granitoids in the eastern North China Craton: Making a Neoarchean upper continental crust during micro-continental collision and post-collisional extension

Chao Wang[1], Shuguang Song[1,*], Yaoling Niu[2,3], Chunjing Wei[1], Li Su[4]

[1] *MOE Key Laboratory of Orogenic Belts and Crustal Evolution, School of Earth and Space Sciences, Peking University, Beijing 100871, China*

[2] *Department of Earth Sciences, Durham University, Durham DH1 3LE, UK*

[3] *Institute of Oceanology, Chinese Academy of Science, Qingdao 266071, China*

[4] *Institute of Earth Sciences, Chinese University of Geosciences, Beijing 100083, China*

Revised manuscript for *Journal of Petrology*

*corresponding author

Shuguang Song

sgsong@pku.edu.cn

ABSTRACT

As the major component, Archean granitoids provide us with an insight into the formation of the early continental crust. In this paper, we report the study of a series of Neoarchean granitoids, including TTG (tonalite, trondhjemite and granodiorite) and potassic granitoids, in the Xingcheng region of the eastern North China Craton. Zircon U-Pb dating shows that the TTG granitoids were emplaced in the Neoarchean within a 75 Myr period (2595-2520 Ma), with coeval mafic magmatic enclaves, followed by intrusion of potassic granitoids. The geochemistry of the TTG granitoids is consistent with partial melting of Mesoarchean enriched mafic crustal sources at different depth levels (up to 10-12 kbar) during a continental collision event. The potassic granitoids are derived from either low-degree melting of Mesoarchean enriched mafic crustal sources or re-melting of Mesoarchean TTGs in response to post-collisional extension, and hybridized with Neoarchean mantle-derived mafic melts by various degrees. The TTG and potassic granitoids in the Xingcheng region record the evolution from collision of micro-continental blocks to post-collisional extension, consistent with other studies, suggesting that the amalgamation of micro-continental blocks is what gave rise to the cratonization of the North China Craton at the end of the Archean. The rock assemblage of these granitoids resembles the syn- and post-collisional magmatism in the Phanerozoic orogenic belt, and the estimated average composition is similar to that of the present-day upper continental crust, suggesting that a proto-type upper continental crust might have been developed at the end of the Archean by a mixture of TTG and potassic granitoids. Together with the prevailing concurrent high-grade metamorphism in the North China Craton, we thus conclude that collisional orogenesis is responsible for the continental cratonization at the end of Archean in

40 the North China Craton.

41 **Keywords:** TTG and potassic granitoids; cratonization at the end of Archean; micro-continental

42 collision; proto-type upper continental crust; the North China Craton.

43

INTRODUCTION

Our knowledge of when and how the mature continental crust may have developed remains incomplete. As the main components of Archean terranes or primary architecture of the continental crust, sodic granitoids of varying composition collectively called the tonalite-trondhjemite-granodiorite (TTG) suites have been extensively studied with the aim of understanding the evolution of the Earth and constraining the differentiation processes of the continental crust (Barker *et al.*, 1979; Jahn *et al.*, 1981; Martin, 1999; Smithies, 2000; Condie, 2005b, 2014; Martin *et al.*, 2005; Moyen, 2011; Moyen & Martin, 2012). Many studies suggest that TTGs are generated by partial melting of mafic rocks under either amphibolite facies (less than 15 kbar; e.g., Foley *et al.*, 2002) or eclogite facies (more than 15-20 kbar; e.g., Rapp *et al.*, 2003) conditions. The compositional similarity between the Archean TTGs and the Phanerozoic subduction-related adakites (e.g., Defant & Drummond, 1990; Castillo, 2012) has led to the popular acceptance that the TTGs may have formed in Archean-type subduction settings (e.g., Condie, 2005b; Martin *et al.*, 2005; Niu *et al.*, 2013). Potassic granitoids are also an important component and closely associated with the TTGs, especially in the Neoarchean terranes. They have been previously interpreted as products of re-melting of pre-existing TTGs (Sylvester, 1994; Moyen *et al.*, 2001, 2003; Bleeker *et al.*, 2003; Whalen *et al.*, 2004; Watkins *et al.*, 2007), and as the marker for the final consolidation of the cratonic continental crust (Frost *et al.*, 1998; Whalen *et al.*, 2004; Martin *et al.*, 2005). However, the role of the potassic granitoids in the growth of the continental crust has been less studied than TTGs.

The present-day upper continental crust is relatively rich in K_2O and HREEs (K_2O/Na_2O = 0.86, $(La/Yb)_N$ = 11; Rudnick & Gao, 2003), and much different from the Archean TTGs

66 ($K_2O/Na_2O = 0.35$, $(La/Yb)_N = 32$; Moyen & Martin, 2012). It is thus important to explore how
67 the present-day upper continental crust may have evolved from the Archean TTG-dominated
68 upper continental crust over the Earth's history. Condie (1993, 2014) proposed that after the
69 Archean the TTG-dominated upper continental crust was gradually replaced by other calc-
70 alkaline granitoids with geochemical features distinct from Archean TTGs, to reach a mature
71 present-day upper continental crust. As there are coeval calc-alkaline granitoids and TTGs
72 reported in some Archean terranes (e.g., Samsonov *et al.*, 2005) and potassic granitoids are
73 widely distributed in Archean cratons worldwide (Bleeker *et al.*, 2003; Moyen *et al.*, 2003),
74 there exists the possibility that in some cases the Archean upper continental crust might have
75 already possessed the present-day upper continental crust composition.

76 The formation and evolution of the North China Craton (NCC) has been the focus of
77 research for decades with extensive investigations carried out to decipher its Precambrian
78 history (e.g., Zhao *et al.*, 1998, 1999, 2001, 2005; Zhai *et al.*, 2010; Nutman *et al.*, 2011; Zhai
79 & Santosh, 2011; Zhao & Cawood, 2012;). The widely distributed Neoarchean to
80 Paleoproterozoic igneous rocks of the NCC offer insights into its Archean to Paleoproterozoic
81 crustal growth and its geodynamic evolution (e.g., Compston *et al.*, 1983; Jahn & Ernst, 1990;
82 Kröner *et al.*, 1998; Yang *et al.*, 2008). However, the geodynamic regime of the NCC during
83 the Neoarchean remains controversial; some researchers suggested a mantle plume-related
84 setting (e.g., Zhao *et al.*, 2001, 2005; Yang *et al.*, 2008), while others argued for a subduction-
85 related environment (e.g., Liu *et al.*, 2010, 2011; Nutman et al., 2011; Wan *et al.*, 2010, 2011;
86 Wang *et al.*, 2011, 2012, 2013).

87 In this study, we present results of in-situ zircon U-Pb dating, bulk rock geochemistry and

Nd isotopes, and in-situ zircon Hf isotopes for the TTG granitoids and their mafic magmatic enclaves (MMEs) as well as the associated potassic granites in the eastern NCC. We show that these granitoids are products of partial melting of proto-crust during micro-continental collision and post-collisional extension at the end of the Archean. Therefore, a proto-type upper continental crust might have been already developed by the end of the Archean in the NCC.

REGIONAL GEOLOGY

The NCC is the largest and oldest craton in China and preserves records of ≥ 3.8 Ga crustal remnants (Liu *et al.*, 1992; Song *et al.*, 1996; Wan *et al.*, 2005). It is suggested to have formed by collision between the Eastern Block and the Western Block along the Trans-North China Orogen (TNCO) at ~1.85 Ga (Fig 1a; Zhao *et al.*, 2001, 2005; Guo *et al.*, 2002) or at ~1.95 Ga as argued by Qian *et al*. (2013), Zhang *et al*. (2013) and Wei *et al*. (2014). The Eastern Block underwent Paleoproterozoic intra-continental rifting along its eastern continental margin in the period of 2.2-1.9 Ga and the rift system was finally terminated by subduction and continental collision at ~1.9 Ga, leading to the formation of the Jiao-Liao-Ji Belt (Fig 1a; Li & Zhao, 2007; Tam *et al.*, 2011). The Western Block comprises two Archean micro blocks, i.e., the Yinshan Block in the north and the Ordos Block in the south, which were amalgamated along the east-west trending Khondalite Belt at ~1.95 Ga (Fig 1a; Santosh *et al.*, 2007a, 2007b; Zhao *et al.*, 2010).

The exposures of the Precambrian basement rocks of the Eastern Block are shown in Fig 1a; except for a few outcrops in the central part (Western Shandong and Eastern Shandong), and mainly distributed in the northern part as three major regions: Jidong (Eastern Hebei),

Northern Liaoning-Southern Jilin and Western Liaoning. These Archean terranes contains ~ 3.8 Ga tonalites (Song *et al.*, 1996; Wan *et al.*, 2005) and experienced a complicated evolution history from 3.8 to 2.5 Ga (Nutman *et al.*, 2011; Zhai & Santosh, 2011).

Our study area is in the northwestern part of the Eastern Block, one of the key regions with the well-exposed Precambrian basement rocks of the NCC (Fig 1a). It mainly consists of the Jidong-Jianping high-grade gneissic terrane with varying protoliths and metamorphic ages (2.6-2.5 Ga; Kröner *et al.*, 1998; Zhao *et al.*, 2001, 2005; Nutman *et al.*, 2011) and the Suizhong granitic terrane (e.g. Yang *et al.*, 2008) with some low to medium-grade greenstone in the Fuxin region (Fig 1b; Liu *et al.*, 2010; Wang *et al.*, 2011, 2012, 2015b). They are partially obscured by Paleoproterozoic to Paleozoic platform strata and Mesozoic volcano-sedimentary sequences, and intruded by Late Paleozoic to Mesozoic igneous rocks.

The Suizhong granitic terrane, previously termed as "Suizhong granitoids", is dominated by granitoids with the TTG assemblage plus minor monzogranite and potassic granite (Figs 1b and c). However, their precise ages and geochemical characteristics have not been well studied. The Qinhuangdao granitoid in the southern part of the Suizhong granitic terrane has long been treated as part of the Eastern Hebei Archean terrane, which has a rock assemblage of diorite, granodiorite and monzogranite emplaced at 2526-2515 Ma and metamorphosed at 2500-2490 Ma with younger K-feldspar granite (2440 Ma) (Fig 1b; Nutman *et al.*, 2011; Yang *et al.*, 2008).

FIELD OCCURRENCE AND SAMPLES

The Xingcheng region lies in the central part of the Suizhong granitic terrane, which has been covered by late sedimentary rocks in places. Several outcrops of the Neoarchean granitoids are

exposed along the west coast of the Bohai Sea (Fig 1b). Samples of this study were collected from four representative locations: Taili, Xingcheng, Juhuadao and Huludao (Fig 1c). The lithologies present in these four representative locations include gneissic granites, tonalites, trondhjemites, granodiorites with mafic magmatic enclaves (MMEs), red-colored potassic granites and locally red pegmatite dykes, which enclose almost all the rock types observed within the Suizhong granitic terrane. Due to the heavy sedimentary covers, the field relationships between most of these lithologies are difficult to determine and map on outcrop scales. Nevertheless, study on samples from these representative outcrops can provide insightful information about the petrogentic history of the Suizhong granitic terrane.

Taili gneissic tonalite-granites

All the Archean granitoids in Taili are strongly deformed with E-W foliations. They are intruded by 230-220 Ma adakitic plutons (Wang *et al.*, 2015a), 155 Ma undeformed granites (our unpublished data) and as yet undated mafic dykes (Fig 2a). The adakitic plutons show the same deformation character as their intruded gneisses (Fig 2a), indicating that the Taili Archean granitoids have experienced latest deformation between 220 Ma and 155 Ma.

Two Archean rock types have been identified in Taili: (1) gneissic tonalites and (2) porphyritic gneissic granites, which are interleaved with each other (Fig 2b). The gneissic tonalites are dark-grey, homogeneous and medium- to fine-grained without porphyroblasts. This rock type has a mineral assemblage of plagioclase (50–60 %), K-feldspar (10-20 %), quartz (10-20 %), amphibole (~ 5 %), minor biotite and accessory zircon, magnetite and titanite. The porphyritic gneissic granites are pale grey, medium- to coarse-grained with feldspar phenocrysts,

and are composed of K-feldspar (40-50 %), plagioclase (20-30 %), quartz (20-30 %), amphibole (~ 5 %), minor biotite and accessory zircon, magnetite and titanite. Strongly deformed mafic dyke (sills) are present (Fig. 2b), but difficult to sample.

Xingcheng porphyritic tonalite-trondhjemites and potassic granites

The tonalite-trondhjemites in Xingcheng are grey, medium- to coarse-grained with plagioclase phenocrysts and contain some MMEs and syn-plutonic dykes. They show porphyritic texture and consist of quartz, plagioclase, K-feldspar, minor hornblende and accessory zircon, magnetite and titanite (Figs 2c-f). The MMEs are dark grey to black and irregular in shape, ranging in size from several to tens of centimeters, with relatively clear boundaries but no chilled margins (Figs 2c-e). They show fine- to medium-grained texture with plagioclase phenocrysts, and their matrix consists of hornblende, plagioclase, minor biotite and accessory zircon, magnetite and titanite. The syn-plutonic dykes show darker color than, and display clear boundaries with their host, together with the irregularly layered-like MMEs, indicating a cumulate origin (Fig 2e). The tonalite-trondhjemites were intruded by later potassic granites with sharp intrusive contacts (Fig 2f). The potassic granites are pinkish red, medium- to coarse-grained and are composed of quartz, K-feldspar, minor biotite and accessory zircon, magnetite and titanite. Both tonalite-trondhjemites and potassic granites are intruded by parallel, red-colored pegmatite dykes (Figs 2e and f).

Juhuadao granodiorites

The granodiorites in Juhuadao are pale grey in color with medium- to coarse-grain size and also contain MMEs. They are intruded by Mesozoic plutons (Fig. 1c). The granodiorites have the

mineral assemblage of quartz, plagioclase, hornblende, minor K-feldspar and accessory zircon, magnetite and titanite. The MMEs are fine- to medium-grained with the mineral assemblage of hornblende, plagioclase, minor biotite and accessory zircon, magnetite and titanite, showing clear contact with the host granodiorites (Fig 2g).

Huludao potassic granites

The potassic granites in Huludao show pinkish red color, fine- to medium-grained texture and are dominated by quartz, K-feldspar, minor biotite and accessory zircon, magnetite and titanite. They are unconformably overlain by the Paleoproterozoic sedimentary rocks of the Changcheng formation (Pt_{2c}) (Figs 1c and 2h).

ANALYTICAL TECHNIQUES

In-situ zircon U-Pb dating

Zircon grains were extracted from crushed samples by standard heavy-liquid and magnetic techniques, and purified by hand-picking under a binocular microscope. The selected grains were embedded in epoxy resin discs and polished down to about half-sections to expose the grain interiors. Cathodoluminescence (CL) images were acquired using a cathodoluminescent spectrometer (Garton Mono CL3+) equipped on a Quanta 200F ESEM at scanning conditions of 15 kV and 120 nA at Peking University.

Measurements of U, Th and Pb in zircons were carried out on an Agilent-7500a quadrupole inductively coupled plasma mass spectrometer coupled with a New Wave UP-193 solid-state laser-ablation system (LA-ICP-MS) in the Geological Lab Center, China University of

Geosciences, Beijing (CUGB) following the analytical procedures in Song *et al*. (2010a). Laser spot size of 36 μm, laser energy density of 8.5 J/cm^2 and a repetition rate of 10 Hz were applied for analysis. The ablated sample material was carried into the ICP-MS by high-purity Helium gas. NIST 610 glass and Harvard standard zircon 91500 (Wiedenbeck *et al.,* 1995) were used as external standards, Si as the internal standard and the standard zircon TEMORA (417 Ma) from Australia (Black *et al.,* 2003) as secondary standard. The software GLITTER (ver. 4.4, Macquarie University) was used for data reduction. The common lead correction was done following Andersen (2002). Age calculations and plots of concordia diagrams were made using Isoplot (ver. 3.0) (Ludwig, 2003).

Bulk rock major and trace element analyses

All the samples are fresh cuttings away from late veinlets with surface contaminants trimmed off before being thoroughly cleaned. Fresh portions of the trimmed samples were crushed to 1-2 cm size chips using a percussion mill. These rock pieces were then ultrasonically cleaned in Milli-Q water, dried and powdered in a thoroughly cleaned agate mill to 200 mesh in the clean laboratory at the Langfang Regional Geological Survey, China.

Bulk rock major and trace element analysis was done at CUGB following Song *et al.* (2010b). Major elements were analyzed on a Leeman Prodigy inductively coupled plasma-optical emission spectroscopy (ICP-OES) system with high dispersion Echelle optics. Based on USGS (US Geological Survey) rock standards AGV-2 and W-2, and CNGR (Chinese National Geological Reference) materials GSR-1 and GSR-3, the analytical precisions (1σ) for most major element oxides are better than 1% with the exception of TiO_2 (~1.5%) and P_2O_5 (~2.0%).

Loss on ignition (LOI) was determined by placing 1 g of samples in a furnace at 1000 °C for a few hours and then reweighting the cooled samples.

Bulk rock trace elements were analyzed using an Agilent-7500a quadrupole inductively coupled plasma mass spectrometry (ICP-MS). About 35 mg powder of each sample was dissolved in distilled acid mixture (1:1 HF + HNO_3) with Teflon digesting vessels and heated on a hot-plate at 195 °C for 48 hours using high-pressure bombs for digestion/dissolution. The sample was then evaporated to incipient dryness, refluxed with 1 mL of 6 N HNO_3 and heated again to incipient dryness. The sample was again dissolved in 2 mL of 3 N HNO_3 and heated at 165 °C for further 24 hours to guarantee complete digestion/dissolution. The sample was finally diluted with Milli-Q water to a dilution factor of 2000 in 2 % HNO_3 solution for analysis. Rock standards USGS AGV-2, W-2 and BHVO-2 were used to monitor the analytical accuracy and precision. Analytical accuracy, as indicated by relative difference between measured and recommended values is better than 5% for most elements, and 10 ~ 15% for Cu, Zn, Gd, and Ta.

Bulk rock Nd isotope analyses

Separation and purification of Nd were done using conventional two-column ion exchange procedures in the ultraclean laboratory of MOE Key Laboratory at Peking University. Approximately 250 mg powder of each sample was dissolved with distilled acid mixture (HF + $HClO_4$) in a sealed Savillex beaker on a hot-plate for 168 hours. The ion exchange procedures include (1) a group separation of light REE through a cation-exchange column (1×7.5 cm^2, packed with 200 mesh AG50W resin); and (2) a purification of Nd through a second cation-

exchange column(0.5×5.5 cm^2, packed with 200 mesh P507 resin), conditioned and cleaned with dilute HCl. Nd isotopic ratios were measured using a Thermo-Finnigan Triton thermal ionization mass spectrometer (TIMS) at the Isotope Laboratory of Tianjin Institute of Geology and Mineral Resources. The $^{147}Sm/^{144}Nd$ ratios were calculated using ICP-MS analyzed Sm and Nd concentrations. Mass fractionation was corrected for by normalizing the measured $^{143}Nd/^{144}Nd$ against $^{146}Nd/^{144}Nd$ ratio of 0.7219. Rock standard USGS BCR-2 was used to evaluate the separation and purification process of Nd, which yielded weighted mean $^{143}Nd/^{144}Nd$ ratio of 0.512632 ± 4 (2σ, n = 100). In order to monitor the data quality during the period of data acquisition, LRIG Nd standard was analyzed and gave a weighted mean $^{143}Nd/^{144}Nd$ ratio of 0.512206 ± 6 (2σ, n = 100).

In-situ zircon Hf isotope analyses

In-situ zircon Lu-Hf isotope analysis of dated samples from the Xingcheng region was carried out using a Neptune multi-collector ICP-MS attached with a New Wave UP-213 laser-ablation system (LA-MC-ICP-MS) at MLR Key Laboratory of Metallogeny and Mineral Assessment, Institute of Mineral Resources, Chinese Academy of Geological Sciences, Beijing. Analytical details are given in Hou *et al*. (2007) and Wu *et al*. (2006). Laser spot size of 40 μm was adopted for analysis and Helium gas was used as carrier gas to transport the laser ablated sample from the laser-ablation cell to the ICP-MS torch via a mixing chamber mixed with Argon gas. Correction for the isobaric interferences of ^{176}Lu and ^{176}Yb on ^{176}Hf was after Hou *et al*. (2007) and Wu *et al*. (2006). Before the analysis, standard zircons (TEMORA, GJ1 and FM02) were analyzed and the efficacy of the correction method of isobaric interferences in Hou *et al*. (2007)

and Wu *et al*. (2006) was tested to be efficient. Zircon GJ1 was used as the reference standard to monitor data quality during analysis, giving a weighted mean $^{176}Hf/^{177}Hf$ ratio of 0.282007 ± 7 (2σ, n=36), which is in accordance with the weighted mean $^{176}Hf/^{177}Hf$ ratio of 0.282000 ± 5 (2σ) measured by the solution analysis method (Morel *et al*., 2008).

RESULTS

Geochronology

Eight samples were selected for zircon U-Pb analysis, including gneissic granite (10TL13), tonalite-trondhjemite (10XC02), granodiorite (12XC22 and 12XC28), MME (11XC03 and 12XC15) and potassic granite (10XC05 and 10XC08) from the four outcrops in the Xingcheng region: Taili, Xingcheng, Juhuadao and Huludao (see Fig 1c for sampling locations). The CL images of representative zircons are shown in Fig 3 and the in-situ LA-ICP-MS U-Pb data are given in Table 1 and plotted in Fig 4.

Zircon grains from all the eight dated samples are euhedral/prismatic, and have varying size (50-250 μm) with length/width ratio of 2:1-5:1. They show typical oscillatory growth zoning of magmatic origin in cathodoluminescent (CL) images (Fig 3), suggesting that these zircons from the granitoids and their MMEs were crystallized from magmas parental to these host rocks. Most of the zircon grains have Th/U ratios varying from 0.3 to 1.8, a few less than 0.3 possibly due to late-stage alteration.

Taili gneissic tonalite-granites

Sample 10TL13 is a gneissic granite from Taili (Figs 1 and 2a-b). U-Pb analysis for twenty-five

zircon grains yields $^{207}Pb/^{206}Pb$ ages ranging from 2581 ± 21 to 2525 ± 21 Ma (1σ) apart from 2 strongly discordant ages due to lead loss (2285 ± 47 and 2463 ± 47 Ma) (Table 1). They form a discordant line with an upper intercept age of 2558 ± 16 Ma (MSWD = 0.50) (Fig 4a). Nineteen analyses on or close to the concordia give a weighted mean $^{207}Pb/^{206}Pb$ age of 2551 ± 9 Ma (MSWD = 0.53), which is in accordance with the upper intercept age. Therefore, the Taili gneissic granites were emplaced at ~2558 Ma.

Xingcheng tonalite-trondhjemites and MMEs

Sample 10XC02 is a tonalite from Xingcheng (Figs 1 and 2c-f). Twenty-five zircon grains were analyzed and have a wide $^{207}Pb/^{206}Pb$ age range of 2578 ± 22 to 2388 ± 23 Ma (1σ) (Table 1). They fall on a discordant line with an upper intercept with concordia at 2559 ± 23 Ma (MSWD = 0.88) (Fig 4b). Seven near-concordant analyses of zircon grains give a weighted mean $^{207}Pb/^{206}Pb$ age of 2548 ± 17 Ma (MSWD = 1.05), agreeing well with the upper intercept age. Thus, the Xingcheng tonalite-trondhjemites crystalized at ~2559 Ma.

Sample 11XC03 is an MME hosted in the Xingcheng tonalite-trondhjemites (Figs 2c-e). Ten zircon grains were analyzed to give a $^{207}Pb/^{206}Pb$ age range of 2487 ± 27 to 2236 ± 26 Ma (1σ) (Table 1). They are extremely discordant due to lead loss and lie along a discordant line under the concordia with a projected upper intercept age of 2546 ± 55 Ma (MSWD = 0.61) (Fig 4c). Thus, the crystalization age of the MMEs in Xingcheng is ~2546 Ma and coeval with the host tonalite-trondhjemites within error.

Juhuadao granodiorites and MMEs

Sample 12XC22 is a granodiorite from Juhuadao (Figs 1 and 2g). Thirty zircon grains were

analyzed to give a wide $^{207}Pb/^{206}Pb$ age range of 2660 ± 17 to 2145 ± 18 Ma (1σ) due to lead loss (Table 1). They define a discordant line and intercept the concordia at 2595 ± 14 Ma (MSWD = 1.20), which is in accordance with the weighted mean $^{207}Pb/^{206}Pb$ age of 9 analyses indistinguishable from concordia (2587 ± 11 Ma; MSWD = 0.86) (Fig 4d). Another granodiorite sample 12XC28 was also selected for dating. Thirty zircon grains were analyzed to give a wide $^{207}Pb/^{206}Pb$ age range of 2582 ± 24 to 1822 ± 58 Ma (1σ) resulting from lead loss (Table 1). They are strongly discordant and form a discordant line intercepting the concordia at 2573 ± 28 Ma (MSWD = 2.90) (Fig 4e). Therefore, the emplacement timing of the Juhuadao granodiorites is between 2595 and 2574 Ma.

Sample 12XC15 is an MME hosted in the Juhuadao granodiorites (Fig 2g). Twenty-four zircon grains were analyzed and give a wide $^{207}Pb/^{206}Pb$ age range of 2583 ± 26 to 1626 ± 95 Ma (1σ) showing effects of lead loss (Table 1). They fall on a discordant line with an upper intercept age of 2568 ± 13 Ma (MSWD = 2.80) (Fig 4f). Thus, the MMEs crystalized at ~2568 Ma, also coeval with the hosting granodiorite within error.

Xingcheng and Huludao potassic granites

Sample 10XC05 is a potassic granite intruding the Xingcheng tonalite-trondhjemites (Figs 1 and 2f). Fifteen zircon grains were analyzed to give a $^{207}Pb/^{206}Pb$ age range of 2573 ± 16 to 2327 ± 15 Ma (1σ) in addition to two strongly discordant ones due to lead loss (1985 ± 51 and 2021 ± 15 Ma) (Table 1). They define a discordant line intercepting the concordia at 2545 ± 20 Ma (MSWD = 0.98) (Fig 4g), in accordance with the weighted mean $^{207}Pb/^{206}Pb$ age of 8 analyses (2531 ± 23 Ma; MSWD = 2.7) near or close to the concordia. Therefore, the

crystallization age of the Xingcheng potassic granites is ~2545 Ma and slightly younger than that of the intruded tonalite-trondhjemites, which is consistent with the field observations of their relative ages (Fig 2f).

Sample 10XC08 is a potassic granite from Huludao (Figs 1 and 2h). Nineteen zircon grains were analyzed to give a $^{207}Pb/^{206}Pb$ age range of 2544 ± 41 to 2334 ± 19 Ma (1σ) (Table 1). They are also strongly discordant and define a discordant line intercepting the concordia at 2520 ± 25 Ma (MSWD = 1.04) (Fig 4h). Therefore, the crystallization ages of the potassic granites in the Xingcheng region range from 2545 Ma to 2520 Ma.

In summary, the emplacement age of Neoarchean granitoids in the studied region is between 2595 and 2520 Ma. The TTG granitoids were emplaced during 2595-2558 Ma, which is coeval with the hosted MMEs of 2568-2546 Ma, followed by intrusion of potassic granites at 2545-2520 Ma.

Geochemistry

Bulk rock major and trace elements

Forty-eight fresh or least altered samples from the four representative outcrops of Neoarchean granitoids in the Xingcheng region, including gneissic granites, tonalite-trondhjemites, granodiorites, MMEs and potassic granites, were selected for bulk rock major and trace element analyses, and the data are reported in Table 2. They vary in composition from dioritic to granodioritc, to quartz monzonitic and to granitic. Most of them are sub-alkaline, with some samples plotted in the alkaline field (Fig 5a).

Taili gneissic tonalite-granites. The gneissic granite samples from Taili are characterized by

enriched K_2O over Na_2O (K_2O/Na_2O = 0.96-2.41) and total alkaline contents (Figs 5a, 5d and 6a) and show a relatively large compositional range in terms of other major elements (Table 2; Figs 5 and 6). They are all metaluminous plotting in the granite field in the An-Ab-Or diagram (Table 2; Figs 5b and c). The Taili gneissic granite samples with lower SiO_2 contents have elevated P_2O_5 and TiO_2 contents (Figs 6b and c). They also have low concentrations of Cr and Ni but relatively high Y and variable Sr abundances (Table 2; Fig 6e and f). They are all enriched in light rare earth elements (LREEs) with varying $(La/Yb)_N$ ratios of 8-51 (Table 2; Fig 12a). They have obvious negative Eu anomalies (Eu/Eu* = 0.50-0.93) and super-chondritic heavy rare earth element (HREE) contents (Fig 7a). In the primitive mantle (PM)-normalized trace element diagram (Fig 8a), they are relatively enriched in large ion lithophile elements (LILEs; e.g., Cs, Rb, Ba and Th) with limited variation and depleted in high field strength elements (HFSEs; negative Nb and Ta anomalies, but no Zr and Hf depletion). They also show a large range of Sr/Y ratios of 7-62 (Fig 12b).

The Taili gneissic tonalite samples have relatively high SiO_2 and K_2O/Na_2O (0.71-0.82) (Table 2; Fig 5d). They are all metaluminous and fall near the TTG field in the An-Ab-Or diagram (Table 2; Figs 5b and c). They also have low concentrations of Cr, Ni and Y but relatively high Sr (Table 2; Fig 6e and f). They show typical fractionated REE patterns of TTGs (or adakites), with high $(La/Yb)_N$ ratios of 72-74 without negative Eu anomalies (Eu/Eu* = 1.11-1.19) (Table 2; Fig 7a). In the PM-normalized trace element diagram (Fig 8a), they are enriched in LILEs, with significant negative anomalies of some HFSEs (e.g., Nb, Ta and Ti) without Zr and Hf depletion. They have positive Sr anomalies with high Sr/Y ratios of 161-172 (Fig 12b).

360 *Xingcheng tonalite-trondhjemites and MMEs.* The tonalite-trondhjemite samples from
361 Xingcheng are intermediate to felsic (Table 2). They are relatively enriched in Na_2O relative to
362 K_2O (K_2O/Na_2O = 0.20-0.67) (Fig 5d), and all plot in or near the trondhjemite field in the An-
363 Ab-Or diagram (Fig 5b). They also have low Cr, Ni and Y, but relatively high Sr (Table 2; Figs
364 6e and f). They are uniform in REE patterns with moderate depletion in HREEs ($(La/Yb)_N$ =
365 25-47) and weakly negative to positive Eu anomalies (Eu/Eu* = 0.76-1.16) (Fig 7b). In the PM-
366 normalized trace element diagram (Fig 8b), they are enriched in LILEs and depleted in Nb, Ta
367 and Ti and show positive Sr anomalies with high Sr/Y ratios of 83-145 (Fig 12b).

368 The MMEs hosted within the Xingcheng tonalite-trondhjemites are mafic to intermediate
369 in composition (Table 2). In contrast with their host, the MMEs have higher TiO_2, Al_2O_3, total
370 Fe_2O_3, MgO, CaO, similar Cr, Ni, Sr, and K_2O/Na_2O (0.42-0.87) (Fig 5d), but lower Ba, Th and
371 U (Table 2; Fig 6). They have higher HREEs with lower $(La/Yb)_N$ ratios of 11-13 than their host
372 and show weakly negative Eu anomalies (Eu/Eu* = 0.68-0.94) (Fig 7b). In the PM-normalized
373 trace element diagram (Fig 8b), the MMEs are relatively depleted in some LILEs (e.g., Ba and
374 Th) and show depletion of HFSEs with negative anomalies of Nb, Zr, Hf and Ti and moderate
375 positive Sr anomalies with relatively high Sr/Y ratios of 39-86 (Fig 12b).

376 *Juhuadao granodiorites and MMEs.* The granodiorite samples from Juhuadao are
377 compositionally intermediate to felsic (Table 2) and with high Na_2O and thus lower K_2O/Na_2O
378 (0.32-0.76), similar to the Xingcheng tonalite-trondhjemites (Table 2; Fig 5d). They fall in the
379 tonalite-trondhjemite-granodiorite field in the An-Ab-Or diagram (Fig 5b). They have
380 intermediate Y and Sr abundances. They are all enriched in LREEs with significantly varying
381 HREE depletion, thus giving varying $(La/Yb)_N$ (8-50) (Fig 7c). They have varrying Eu/Eu*

(0.67-1.29) and an inverse Yb-SiO_2 correlation (Table 2; figure not shown). In the PM-normalized trace element diagram (Fig 8c), they are enriched in LILEs and depleted in Nb, Ta and Ti with varying Sr/Y ratios (19-57; Fig 12b).

The MMEs in the Juhuadao granodiorites are mafic with relatively low SiO_2 and high K_2O/Na_2O (0.41-0.62), consistent with the host granodiorite (Table 2; Fig 5d). They have low TiO_2, MgO, Cr, Ni, and Sr (Table 2; Fig 6). In contrast with their host, they have flat LREE patterns with high HREEs and thus weak REE fractionation ($(La/Yb)_N = \sim 4$), lower Sr/Y ratios (12-15) with no obvious Eu anomaly (Figs 7c and 12b). In the PM-normalized trace element diagram (Fig 8c), they are depleted in some LILEs (e.g., Th and U) and have negative anomalies of HFSEs (Nb, Ta, Zr, Hf and Ti).

Xingcheng and Huludao potassic granites. The potassic granites intruding the Xingchegn tonalite-trondhjemites have high SiO_2, and are metaluminous to slightly peraluminous (Table 2; Fig 5c), enriched in K_2O (K_2O/Na_2O = 1.50-1.78; Fig 5d), and fall in the granite field in the An-Ab-Or diagram (Fig 5b). They have relatively low Cr, Ni, Y and Sr concentrations (Table 2; Figs 6e and f). They show fractionated REE patterns ($(La/Yb)_N$ = 18-24) with negative Eu anomalies (Eu/Eu* = 0.52-0.74) and concave HREE patterns (Fig 7d). In the PM-normalized trace element diagram (Fig 8d), they are enriched in LILEs and depleted in some HFSEs such as Nb and Ti but with no depletion of Zr and Hf. Also shown is the depletion of Sr with moderate Sr/Y ratios of 13-48 (Fig 12b).

The potassic granite samples from Huludao are peraluminous (Fig 5c) and are strongly enriched in K_2O with elevated K_2O/Na_2O (1.17-23.04; Fig 5d). They have low Cr, Ni, Y and Sr abundaces (Table 2; Figs 6e and f). They have fractionated REE patterns ($(La/Yb)_N$ = 21-46)

and negative Eu anomalies (Eu/Eu* = 0.74-0.95), with HREE patterns being flat to concave (Fig 7d). In the PM-normalized trace element diagram (Fig 8d), they are enriched in LILEs, and depleted in Nb, Ta and Ti. They are strongly depleted in Sr with moderate Sr/Y ratios of 4-59 (Fig 12b).

Bulk rock Nd isotopic compositions

Bulk rock Sm-Nd isotopic data for the Neoarchean TTG and potassic granitoids in the Xingcheng region are given in Table 3 and plotted in Fig 9. Two Taili gneissic granite samples have uniform initial $^{143}Nd/^{144}Nd$ ratios (0.509320-0.509325) with $\varepsilon_{Nd}(t)$ values of -0.2 and two-stage depleted mantle Nd model ages (T_{DM2}) of 2.91-2.90 Ga. Four Xingcheng tonalite-trondhjemite samples have a narrow range of initial $^{143}Nd/^{144}Nd$ ratios (0.509248-0.509364) with $\varepsilon_{Nd}(t)$ values from -1.6 to -0.6 and two-stage depleted mantle Nd model ages (T_{DM2}) of 3.02-2.84 Ga. The MMEs within the Xingcheng tonalite-trondhjemites exhibit homogeneous initial $^{143}Nd/^{144}Nd$ ratios (0.509261-0.509314) with $\varepsilon_{Nd}(t)$ values of -1.7 to -0.6 and T_{DM2} values of 3.02-2.94 Ga, essentially the same as their host. Four Juhuadao granodiorite samples have initial $^{143}Nd/^{144}Nd$ ratios (0.509167-0.509335) with $\varepsilon_{Nd}(t)$ values from -2.3 to +1.0 and T_{DM2} values of 3.10-2.84 Ga. The MMEs contained within the Juhuadao granodiorites have uniform $^{143}Nd/^{144}Nd$ ratios (0.509295-0.509313) with $\varepsilon_{Nd}(t)$ values of -1.9 to -0.4 and T_{DM2} values of 3.06-2.94 Ga. The Xingcheng potassic granite samples have initial $^{143}Nd/^{144}Nd$ ratios (0.509313-0.509403) with $\varepsilon_{Nd}(t)$ values of -1.4 to +1.0 and T_{DM2} values of 2.97-2.80 Ga. The Huludao potassic granite samples show narrow ranges of initial $^{143}Nd/^{144}Nd$ ratios (0.509313-0.509328) with $\varepsilon_{Nd}(t)$ values of -1.4 to -1.1 and T_{DM2} values of 2.97-2.95 Ga.

Zircon Hf isotopic compositions

Zircon Hf isotopic data for these Neoarchean granitoids are given in Table 4 and plotted in Figs 10 and 11. Zircons of the Taili gneissic granite (sample 10TL13) have narrow ranges of initial $^{176}Hf/^{177}Hf$ ratios (0.281207-0.281277) with $\varepsilon_{Hf}(t)$ values of +2.0 to +7.3 and two-stage depleted mantle Hf model ages (T_{DM2}) of 2.85-2.59 Ga, slightly younger than the Nd model ages. Zircons of the Xingcheng tonalite-trondhjemite (sample 10XC02) have uniform initial $^{176}Hf/^{177}Hf$ ratios of 0.281179-0.281242, $\varepsilon_{Hf}(t)$ values of 1.1 to 3.3 and T_{DM2} values of 2.89-2.79 Ga. Zircons of the Juhuadao granodiorite (samples 12XC22 and 12XC28) show initial $^{176}Hf/^{177}Hf$ ratios of 0.281192-0.281356 with $\varepsilon_{Hf}(t)$ values of 1.9 to 7.7 and T_{DM2} values of 2.87-2.58 Ga. Zircons of the MMEs hosted within the Juhuadao granodiorite (sample 12XC15) have uniform initial $^{176}Hf/^{177}Hf$ ratios of 0.281276-0.281320, $\varepsilon_{Hf}(t)$ values of 4.8 to 6.3 and T_{DM2} values of 2.72-2.65 Ga. Zircons of the Xingcheng potassic granite (sample 10XC05) have homogeneous Hf isotopic compositions with initial $^{176}Hf/^{177}Hf$ ratios of 0.281165-0.281261, $\varepsilon_{Hf}(t)$ values of 0.2 to 3.7 and T_{DM2} values of 2.92-2.76 Ga. Zircons of the Huludao potassic granite (sample 10XC08) have relatively large range of initial $^{176}Hf/^{177}Hf$ ratios from 0.281175 to 0.281301, $\varepsilon_{Hf}(t)$ values from 0.0 to +6.7 and T_{DM2} values of 2.91-2.57 Ga.

DISCUSSION

Petrogenesis of Neoarchean TTG granitoids and MMEs

TTG granitoids: partial melting of Mesoarchean enriched mafic crust at varying depths

Even though exposed in different locations and showing large compositional variation from sodic-rich tonalite-trondhjemite-granodiorite (the Xingcheng tonalite-trondhjemites and the Juhuadao granodiorites) to potassic gneissic tonalite (the Taili gneissic tonalites), the age and isotopic data (Tables 3 and 4; Figs 9-11) suggest that the TTG granitoids in the Xingcheng region were emplaced contemporaneously and thus should share similar magma sources.

The Neoarchean TTG granitoids in the Xingcheng region have relatively high SiO_2 and low MgO, Cr and Ni, indicating a crustal source rather than being directly originated from the mantle (Table 2; Fig 6d). They have bulk rock $\varepsilon_{Nd}(t)$ values of -2.3 to 1.0 and Nd T_{DM2} values of 3.10-2.84 Ga (Table 3 and Fig 9), and their zircons have positive $\varepsilon_{Hf}(t)$ values of 1.1 to 7.7 and Hf T_{DM2} values of 2.89-2.62 Ga (Table 4 and Figs 10 and 11), pointing to a Mesoarchean (3.1-2.9 Ga) crustal sources without the involvement of Paleo- to Eoarchean crustal materials (Fig 11). Additionally, their major element compositions are similar to those of experimental metabasalt melts (Figs 5-6 and 12c). However, Mesoarchean rocks in the eastern NCC are mainly TTGs and no mafic magmatism has been reported so far. Some of the Mesoarchean TTGs are characterized by negative zircon $\varepsilon_{Hf}(t)$ values (e.g., Tiejiashan granites in the Anshan area; Wan *et al.*, 2007; Fig 11), which is consistent with an origin of reworking of Paleo- to Eoarchean crustal materials and cannot act as the sources of the Neoarchean TTG granitoids in

462 the Xingcheng region. Some Mesoarchean TTGs exhibit depleted zircon Hf isotopic
463 compositions (e.g., Mesoarchean TTGs in Eastern Shandong; Liu *et al*., 2013a; Wang *et al*.,
464 2014b; Wu *et al*., 2014; Xie *et al*.; 2014; Fig 11), which are best explained as resulting from
465 melting of mantle-derived basaltic materials of Mesoarchean age. This would point to the
466 existence of Mesoarchean juvenile mafic magmatism in the eastern NCC. Furthermore, the
467 wide range of SiO_2 contents of the Neoarchean TTG granitoids and their MMEs required a
468 mafic precursor instead of felsic sources like TTGs. All these observations and inferences
469 indeed suggest that the Neoarchean TTG granitoids in the Xingcheng region must have derived
470 from Mesoarchean juvenile mafic crustal sources.

471 The Neoarchean TTG granitoids in the Xingcheng region show large major and trace
472 element compositional variation with enrichment of LILEs (e.g., Rb, Ba and Sr) and depletion
473 of HFSEs (e.g., Nb, Ta and Ti) (Figs 5-9). As suggested previously (e.g., Moyen *et al*., 2007,
474 2010), the compositions of TTGs are mainly controlled by the source compositions and the
475 pressures/depths of melting. The enrichment of LILEs (Figs 6a and 8) and relatively higher
476 K_2O/Na_2O of the studied TTG granitoids suggest that their Mesoarchean juvenile mafic sources
477 should be more enriched than those of the typical sodic TTGs (typical Archean TTGs K_2O/Na_2O
478 = 0.35; Moyen & Martin, 2012; Fig 5d). Therefore, the Neoarchean TTG granitoids in the
479 Xingcheng region are predicted to have derived from Mesoarchean mafic crustal rocks that are
480 more enriched than the present-day MORB (EMORB-like?) (Smithies, 2000; Qian & Hermann,
481 2013). An enriched mafic source has also been proposed to explain the compositions of TTGs
482 in other Archean cratons (e.g., Champion & Smithies, 2007; Moyen *et al*., 2007; Smithies *et*
483 *al*., 2009). In addition, most Archean mafic magmatic rocks are characterized by somewhat

484 enriched trace element signatures (Jahn *et al*., 1980; Condie, 2005a; Hollings & Kerrich, 2006;
485 Moyen & Martin, 2012; van Hunen & Moyen, 2012). It should be noted that to accurately
486 determine the nature and the enrichment mechanism of the Mesoarchean enriched mafic crustal
487 rocks is not straightforward because no Mesoarchean mafic magmatism has been reported in
488 the eastern NCC. It is possible that the enrichment reflects a prior mantle source metasomatism
489 caused by recycled even earlier crustal components (Smithies *et al*., 2009).

490 The Xingcheng tonalite-trondhjemites, the Taili gneissic tonalites and some of the
491 Juhuadao granodiorites are characterized by high $(La/Yb)_N$ and Sr/Y ratios and thus plot in the
492 TTG-adakite field in the $(La/Yb)_N$-$(Yb)_N$ and Sr/Y-Y diagrams (Figs 12a and b), suggesting the
493 presence of garnet as a residual phase in the magma source region. They all have positive or
494 slightly negative Eu anomalies and belong to the high-Sr series defined by Moyen *et al*. (2007),
495 implying that there was no or little plagioclase left in the magma sources (Fig 7). In Fig 13, the
496 pressure-controlled ΔX parameters on the vertical axes of these samples suggest that they were
497 formed under higher pressures than other samples, reflecting the presence or absence of some
498 pressure-sensitive minerals such as garnet, plagioclase and rutile in the magma sources (Moyen
499 *et al*., 2010). Thus these samples were most likely derived from mafic crustal sources at
500 relatively high pressures (~10-12 kbar) with garnet and amphibole present as residual phases
501 with little or no plagioclase (Rapp *et al*., 1991; Sen & Dunn 1994; Qian & Hermann, 2013).
502 Geochemical modeling illustrated in Fig 12a shows that they could be generated by 10-25 %
503 partial melting of a mafic crustal source (EMORB-like) with varying proportions of garnet.
504 Thus, the appropriate source lithology for samples with high Sr/Y and $(La/Yb)_N$ ratios is likely
505 to be garnet amphibolite rather than eclogite. These samples should correspond to the medium

506 pressure group of TTGs defined by Moyen (2011).

507 In contrast, other samples of the Juhuadao granodiorites are distinct in having lower Sr,
508 Sr/Y and $(La/Yb)_N$ and higher Y and negative Eu and Sr anomalies (Figs 6e and f), plotting in
509 the field of typical arc rocks in $(La/Yb)_N$-$(Yb)_N$ and Sr/Y-Y diagrams (Figs 12a and b). However,
510 they are similar to samples with high Sr/Y and $(La/Yb)_N$ ratios in terms of major elements and
511 bulk rock Nd and zircon Hf isotopic compositions. Thus, they may be derived from a similar
512 Mesoarchean mafic crustal source, but at lower pressures (< 10 kbar) (Qian & Hermann, 2013),
513 which is further supported by relative positions of these samples compared with their high-
514 pressure counterparts in Fig 13. The obvious negative Eu and Sr anomalies of these samples
515 (Figs 7 and 8) are best explained as the presence of plagioclase as a residual phase during partial
516 melting although the effect of plagioclase crystallization cannot be ruled out. The relatively flat
517 to concave HREE patterns also point to the presence of amphibole as a residual phase.
518 Geochemical modeling illustrated in Fig 12a shows that they could be generated by partial
519 melting of a mafic crustal source (EMORB-like) metamorphosed into garnet-free amphibolite.
520 The appropriate source lithology for these samples with lower Sr/Y and $(La/Yb)_N$ ratios should
521 be amphibolite (Foley *et al.*, 2002), corresponding to a shallower depth and the medium
522 pressure group of TTGs defined by Moyen (2011). Therefore, it is reasonable to conclude that
523 the Neoarchean TTGs in the Xingcheng region resulted from partial melting of an enriched
524 basaltic protolith at varying depths (Moyen, 2011).

525 The bulk rock Nd isotopic compositions of the Neoarchean TTG granitoids in the
526 Xingcheng region have a small range of variation around chondritic values (Table 3; Fig 9),
527 while their zircon Hf isotopic compositions show larger variation from chondritic up to depleted

528 mantle values (Table 4; Figs 10 and 11). Some would explain such differential variation as due
529 to the shorter half-life of ^{176}Lu (36 Ga) relative to the longer half-life of ^{147}Sm (108 Ga) and the
530 variation of Lu/Hf ratios is larger than Sm/Nd ratios during partial melting processes, resulting
531 in the fact that during a given timespan, the variation of $^{176}Hf/^{177}Hf$ is larger than $^{143}Nd/^{144}Nd$
532 (Wu *et al.*, 2007). On the other hand, zircons can record changes of the ambient melts during
533 their growth and crystallization. It is common that zircons have homogeneous U-Pb ages but
534 with heterogeneous Hf isotopic compositions, which is interpreted by some as resulting from
535 replenishment of magmas with distinctively different sources (e.g., Griffin *et al.*, 2002;
536 Belousova *et al.*, 2006; Yang *et al.*, 2008; Zeh *et al.*, 2009). This interpretation advocates open-
537 system magma evolution and most likely reflects the involvement of Neoarchean juvenile
538 mantle-derived melts rather than the contribution of heterogeneous sources as their bulk rock
539 Nd isotopic compositions are considerably homogeneous. In the magmatic process, the bulk
540 rock Nd isotopic compositions of the magmas did not significantly change if the addition of
541 juvenile mantle-derived mafic melts was not obvious, thus the contaminated magmas had bulk
542 rock Nd isotopic compositions similar to the original magmas and the bulk rock Nd isotopic
543 compositions may record more reliable information about the crustal residence time of the
544 source materials (Wan *et al.*, 2015). Juvenile mantle-derived mafic magmatism has been
545 reported to take place in the eastern NCC during the Neoarchean (e.g., Wan *et al.*, 2010; Bai *et*
546 *al.*, 2016 and references therein), which may provide heat to trigger partial melting of the
547 Mesoarchean mafic crustal source for the granitoid magmatism we discuss here, and also
548 contribute to the compositional complexities of our samples (Figs 9-11).

549 In summary, the Neoarchean TTGs in the Xingcheng region were sourced from partial

550 melting of the Mesoarchean lower crustal source at varying depths/pressures heated and
551 contaminated by Neoarchean juvenile mantle-derived mafic magmas.

552 *MMEs: Cumulates resulting from fractional crystallization of the TTG granitoids*

553 The TTG granitoids in the Xingcheng region show large compositional variation (Fig 6), which
554 is likely the combined effect of modal mineralogy variation and fractional crystallization. The
555 slightly concave HREE patterns of some samples indicate that amphibole might be a
556 fractionation phase as well as being a residual phase in the sources (Fig 7). Furthermore, the Sr
557 concentrations show negative correlation with SiO_2, implying the role of plagioclase as a
558 crystallization phase. The 'fan-like' HREE patterns of TTG/adakitic granitoids (Fig 8) were
559 commonly explained as the results of fractional crystallization of garnet-bearing assemblages
560 at high pressures (e.g., Macpherson *et al.*, 2006). However, it is not the case for the TTG
561 granitoids in the Xingcheng region mainly because: (1) there is no increase of Dy/Yb with
562 differentiation (Fig 12d), which should be expected if garnet ($D_{Yb}/D_{Dy} > 1$) was a liquidus phase;
563 (2) crystallization of garnet from TTG magmas needs a high-pressure condition over 14 kbar
564 (e.g., Adam *et al.*, 2012; Hoffmann *et al.*, 2014; Song *et al.*, 2014); and (3) in partial melts
565 (usually tonalitic) of mafic rocks, as calculated by Hoffmann *et al.* (2014), the potential of
566 garnet as a fractional phase is limited. Therefore, low-pressure (< 10 kbar) fractional
567 crystallization of amphibole and plagioclase should contribute to the evolution of the TTG
568 granitoids in the Xingcheng region as evident by the existence of MMEs within them. We
569 performed trace element geochemical modelling of fractional crystallization of amphibole and
570 plagioclase from the TTG granitoid sample with the lowest SiO_2 contents, but as pointed out

by Moyen *et al*. (2007, 2010), fractional crystallization of this assemblage has limited effects on the compositions of the TTG granitoids (results not shown).

MMEs are common in intermediate to felsic granitoids within continental arcs and collisional belts. Different models have been proposed to explain the origin of MMEs, including recrystallized and refractory restite (Chappel *et al.*, 1987, 1999; Chen *et al.*, 2014), inclusion of mafic magma derived from the mantle (Vernon, 1984; Holden *et al*., 1987; Chen *et al.*, 2002; Yang *et al.*, 2007) or early crystalized cumulates (Wall *et al.*, 1987; Niu *et al.*, 2013; Huang *et al.*, 2014; Chen *et al*., 2015). The MMEs hosted in the TTG granitoids in the Xingcheng region are coeval with their host and have almost overlapping bulk rock Nd isotopic compositions (Fig 9), implying a genetic connection. The relatively low contents of MgO, Cr and Ni imply that they were not mantle derived melts. Several observations are supportive of cumulate origin for the MMEs: (1) the MMEs have essentially the same mineral assemblages as their host except for lacking K-feldspar, which is a later liquidus phase and match the predicted low-pressure fractional crystallization assemblage of the TTG granitoids; (2) the MMEs have higher HREE abundances than their hosts and their hosts exhibit fan-shaped REE patterns with the negative Yb-SiO_2 correlation (figure not shown); (3) the MMEs and their host have overlapping and indistinguishable bulk rock Nd and zircon Hf isotopic compositions (Figs 9-11). Therefore, these MMEs are most consistent with an origin of early crystallized cumulates which were mixed into the magma by periodical replenishment of magma and subsequent induced magma convection in the magma chamber (Chen *et al*., 2015, 2016).

Petrogenesis of potassic granitoids#

In most Archean cratons (e.g., the Barberton, Dharwar, Zimbabwe and Slave cratons; Bleeker *et al.*, 2003; Moyen *et al.*, 2003), potassic granitoids are widespread and voluminous and show a great compositional diversity such as CA1-type (Archean calc-alkaline granites formed by partial melting of the mid- to lower continental crust under granulite facies conditions leaving plagioclase and othopyroxene as residual phases), CA2-type (Archean calc-alkaline granites formed by partial melting of the lower continental crust under granulite facies but leaving plagioclase and garnet as residual phases), sanukitoid suite, A-type and S-type (Sylvester, 1994; Jayananda *et al.*, 2006), which then played an important role in balancing the average compositions of the upper continental crust. Such a compositional diversity indicates a variety of processes, such as the involvement of various sources melted at different depths and fractional crystallization.

Three types of potassic granitoids have been recognized in our studied region: (1) the Taili gneissic granites, (2) Xingcheng potassic granites and (3) Huludao potassic granites. Their ages range from 2558 Ma to 2520 Ma. These potassic granitoids could be generated through different scenarios, such as (1) (low-degree?) re-melting of former TTGs, (2) low-degree melting of enriched (EMORB or OIB affinity) mafic crustal sources, (3) low-degree partial melting of an enriched mantle, (4) final products of fractionation crystallization of felsic magmas and (5) high-degree of fractionation of hydrous medium- to high-K basaltic magmas.

It should be noted that the potassic granitoids in the Xingcheng region form linear trends with the TTGs in the Harker diagrams (Fig 6) and have almost indistinguishable bulk rock Nd and zircon Hf isotopic compositions with the TTG granitoids, which points to the possibility

613 that these potassic granites might be the final products of fractionation of the TTG magmas.
614 However, as the gap between formation ages of the TTG granitoids (2595-2558 Ma) and the
615 potassic granites (2545-2520 Ma) is large, it is difficult to envisage that such a long-lived
616 fractionation process of relatively cool and viscous felsic TTG magmas could generate these
617 potassic granites. Potassium-rich felsic melts can also be produced through high degrees of
618 fractionation of hydrous medium- to high-K basaltic magmas especially under high pressures
619 (e.g., Sisson *et al.*, 2005), but the absence of contemporaneous K-rich basaltic magmas in the
620 Xingcheng region and the confined range of SiO_2 contents of these potassic granites preclude
621 this scenario as the generation mechanism of the potassic granites in the Xingcheng region.

622 ### *Taili gneissic granites: melting of Mesoarchean enriched mafic crust at low-*
623 ### *pressure hybridized with Neoarchean mantle-derived mafic melts*

624 The Taili gneissic granties are characterized by relatively high K_2O contents, and are distinct
625 from the TTG granitoids (Fig 6a). In Fig 13, the source composition-controlled ΔX parameters
626 on the horizontal axes of these samples indicate that they should be sourced from a more
627 enriched source compared with that of the TTG granitoids, which is also reflected by their
628 enriched LILE concentrations (Fig 8a). Their bulk rock Nd and zircon Hf T_{DM2} point to a source
629 that was ultimately extracted from the mantle in the Mesoarchean (Table 3 and 4). The Taili
630 high-K gneissic granites have low Y and Sr abundances (Figs 6e and f) and show negative Eu
631 and Sr anomalies (Figs 7a and 8a). Their pressure-controlled ΔX parameters also imply that
632 they should be formed under lower pressures (Fig 13).

633 Some Taili high-K gneiss samples are characterized by low SiO_2 (five samples < 65 wt%),

elevated TiO_2, P_2O_5 and MgO contents (Fig 6b, c and d), as well as higher compatible elements like Cr and Ni (Table 2), which can exclude the possibilities of re-melting of former TTGs and final products of fractionation crystallization of felsic magmas. The coupled enrichment in LILEs and compatible elements strongly indicates the contribution of a component with mantle signatures (Miller *et al.*, 2008), which is also supported by the zircon Hf isotopic composition ($\varepsilon_{Hf(t)} > +2$) of the Taili gneissic granites (Figs 10 and 11). One zircon gives $\varepsilon_{Hf}(t)$ of 7.3 and T_{DM2} of 2588 Ma, implying hybridization of a Neoarchean juvenile mantle-derived magma. The negative but near chondritic $\varepsilon_{Nd}(t)$ values (-0.2) suggest little crustal contamination, if any, not significant. In the $Mg^{\#}$-SiO_2 diagram (Fig 12c), these rocks follow an AFC or magma mixing trend of mantle-derived mafic melts. Therefore, it is reasonable to conclude that the Taili high-K gneissic granites were produced by low-pressure melts of Mesoarchean EMORB/ OIB-like enriched mafic crust with hybridization of Neoarchean juvenile mantle-derived mafic melts. It should be noted that fractional crystallization should also contribute to the compositional variation, but it should be a second-order effect.

Huludao potassic granites: re-melting of Mesoarchean TTGs at low-pressure

The 2520 Ma Huludao potassic granites are characterized by sub-vertical trends in the K_2O-SiO_2 diagram (Fig 6a), and they have relatively high K_2O/Na_2O ratios (Fig 5d) and LILE concentrations (Fig 8d). These potassic granites also define a trend towards a richer source compared with that of the TTG granitoids in Fig 13. Besides, they are all peraluminous with A/CNK ratios of 1.14-1.20 (Fig. 5c). These geochemical features are usually attributed to partial melting of comparatively enriched and relatively potassic sources (Moyen *et al.*, 2007). Like

655 the TTG granitoids, their bulk rock Nd and zircon Hf isotopic compositions point to a source
656 that were extracted from the mantle during Mesoarchean (Table 4). Thus the likely source of
657 these potassic granites might be the Mesoarchean TTGs sourced from juvenile mantle-derived
658 rocks (Fig 11). Based on field and experimental investigations, some researchers proposed that
659 Archean potassic granites result from partial melting of former TTGs and represent within-crust
660 differentiation (Moyen *et al.*, 2001, 2003; Castro, 2003; Whalen *et al.*, 2004; Patiño Douce,
661 2005; Watkins *et al.*, 2007; Xiao & Clemens, 2007). Partial melting of TTGs is usually related
662 to the breakdown of amphibole and biotite, which releases potassium into melts (Watkins *et al.*,
663 2007). However, partial melting of typical sodic TTGs will generate relatively sodic melts and
664 only if the source is potassic TTGs will the partial melts be enriched in K_2O (Patiño Douce &
665 Beard, 1995; Skjerlie & Johnston, 1996; Castro, 2003; Watkins *et al.*, 2007). As estimated
666 above, the TTG granitoids in the Xingcheng region should be sourced from a Mesoarchean
667 enriched mafic crustal sources and it is highly likely that there exist some potassic TTGs derived
668 from these enriched sources. Re-melting of these relatively potassic TTGs would facilitate the
669 generation of the Huludao potassic granites. However, it should be noted that these potassic
670 granites should not be derived from the contemporaneous TTG granitoids as there are no signs
671 of partial melting observed in these TTG granitoids. These potassic granites have lower
672 concentrations of Y and Sr (Figs 6e and f), and are characterized by negative Sr and Eu
673 anomalies (Figs 7d and 8d), implying the presence of plagioclase and the absence of garnet in
674 the sources. Also they show a trend towards lower pressures of melting on Fig 13. Therefore
675 these potassic granites are best explained as their parental melts resulting from relatively low
676 pressure melting. It should be noted that some of the potassic granites have higher $(La/Yb)_N$

and Sr/Y ratios and accordingly plot in the TTG and adakite field in Fig 12a and b. A possible explanation for this feature could be inheritation from their TTG source rocks.

Xingcheng potassic granites: low-degree partial melting of enriched mafic crust

Experimental investigations suggested that low degrees of partial of partial melting (< 20%) of alkali metabasalt could lead to potassic felsic melts (e.g., Sen & Dunn, 1994) as potassium is highly incompatible during partial melting (Qian & Hermann, 2013). The 2545 Ma Xingcheng potassic granites are metaluminous with A/CNK ratios of 0.87-1.06 (Fig. 5c) and have obvious negative Eu anomalies (Fig. 7d). They exhibit distinct geochemical features from the potassic granites in many Archean cratons, i.e., relatively high Sr/Y and $(La/Yb)_N$ ratios and falling in or near the TTG/adakite field in Figs. 12a and b, which are similar to the potassic C-type adakites of mafic crust origin (Rapp *et al.*, 2002). Their MREE-depleted patterns (Fig 7d) are also similar to some post-collisional, potassic granites in the Paleozoic North Qaidam ultrahigh pressure metamorphic belt (Wang *et al.*, 2014a). Besides, they plot in the fields of experimental metabasalt melts, implying that they might be sourced from partial melting of mafic rocks. These potassic granites show concave HREE patterns, implying that amphibole should be left in the residue or as a fractional phase. As illustrated in Fig. 12a, the Xingcheng potassic granites could be generated by low degrees (< 20%) of partial melting of an enriched mafic source metamorphosed to garnet amphibolite with varying proportions of garnet. Importantly, these potassic granites have similar bulk rock Nd and zircon Hf isotopic compositions with those of the coexisting TTG granitoids (Figs 9-11). Therefore, the potassic granites and the TTG granitoids likely share the same Mesoarchean enriched mafic crustal sources. Considering the

698 fact that these potassic granites have fairly high SiO_2 contents (up to 76.11 wt.%), low-degree
699 partial melting of an enriched mafic source might be able to facilitate the generation of the
700 potassic granites in the Xingcheng region. Compared with the Taili gneissic granites, they have
701 a narrow range of high SiO_2 contents, implying limited interaction with Neoarchean mantle-
702 derived mafic melts.

703 Neoarchean magmatism and crustal growth in the NCC

704 Zircon U-Pb dating reveals that the TTG and potassic granitoids in the studied region were
705 emplaced at 2595-2520 Ma, i.e., ~75 Myrs towards the end of the Neoarchean. The age data
706 statistics of the Archean basement rocks in the NCC also show that the Late Neoarchean (2.6-
707 2.5 Ga) is an important period of magmatism (Yang *et al.*, 2009; Geng *et al.*, 2010; Nutman *et*
708 *al.*, 2011; Sun *et al.*, 2012), with widespread TTG suites, ultramafic to mafic igneous rocks and
709 charnockites and granites (Zhao *et al.*, 2001, 2005).

710 The TTG granitoids and potassic granites in the Xingcheng region have bulk rock Nd and
711 zircon Hf model ages ranging between 3.0 and 2.6 Ga (Tables 3 and 4; Figs 10-12), suggesting
712 that no older (> 3.0 Ga) sources were involved in their genesis. All zircons from these rocks
713 have positive $\varepsilon_{Hf}(t)$ and fall between the evolution line of the depleted mantle and the CHUR in
714 the $\varepsilon_{Hf}(t)$-t diagram (Fig 12), distinct from those from the Early Archean rocks in the NCC (Wu
715 *et al.*, 2005a), again pointing to more juvenile crustal sources compared with the Paleo- to
716 Eoarchean crustal sources. Many studies have shown that the Archean basement rocks in the
717 NCC are characterized by Nd and Hf model ages clustering at 3.0-2.6 Ga, indicating the timing
718 of formation of the protoliths or segregation of the parental magma from the mantle (Wu *et al.*,

2005b; Yang *et al.*, 2008, 2009; Geng *et al.*, 2010; Jiang *et al.*, 2010; Wan *et al.*, 2011; Zhai & Santosh, 2011; Shi *et al.*, 2012; Wang & Liu, 2012 and references therein). We thus conclude that significant crustal growth occurred in the NCC during the Neoarchean, corresponding with the global growth of the Earth's crust recognized from other cratons (Condie & Aster, 2010; Condie *et al.*, 2011; Condie & Kröner, 2013; Condie, 2014 and references therein).

It is widely acknowledged that TTGs are the main components of Archean terranes and represent the primary felsic crust of the Earth (Martin *et al.*, 2005; Moyen, 2011), and the average Archean upper continental crust is essentially identical to the Archean TTGs (Condie, 1993, 2005b). However, as mentioned above, there are significant compositional discrepancies between the mature present-day felsic upper continental crust and the Archean TTGs, mainly in potassium, Y and HREEs (Table 5 and Fig 14). These compositional discrepancies were gradually balanced by the addition of calc-alkaline granitoids with higher Y, HREEs and potassium to the Archean upper continental crust throughout the Earth's history, which is reflected by the fact that the volume ratio of TTGs relative to calc-alkaline granitoids has decreased since the end of the Archean (Condie, 2008),

Taking together with the Qinghuangdao granitoids reported by Yang *et al.* (2008), we calculated the compositions of the Neoarchean upper continental crust in the Xingcheng-Qinhuangdao region on the basis of average compositions of TTG granitoids and potassic granites. We have found that the mix of TTG granitoids/potassic granites = 9:1 matches well the present-day upper continental crust with K_2O/Na_2O of 0.86, except that Y and HREE contents are ~ 20-30 % lower than those of the present-day upper continental crust (Table 5 and Fig 14). Therefore, these Neoarchean granitoids in the studied region can make at least 70-80 %

741 of the compositions of the present-day upper continental continent crust, implying that a proto-
742 type upper continental crust of the NCC could be formed at the end of the Archean. It should
743 be noted that this scenario applies to the maturation of the continental crust of the NCC but
744 further study is needed if this is of general significance.

745 Tectonic implications: from micro-continental collision to post-
746 collisional extension

747 The geodynamic setting of the Neoarchean blocks of the NCC, in which extensive magmatism
748 and metamorphism occurred, has long been the subject of research focus and debate. The heat
749 source for widespread regional metamorphism and large-scale partial melting of crustal
750 materials is usually considered to be related to the intrusion and underplating of large volumes
751 of mantle-derived magmas. The emplacement of sufficient amounts of mantle-derived magmas
752 may occur in a variety of environments, including subduction-related settings (e.g., Liu *et al.*,
753 2010, 2011; Wan *et al.*, 2010, 2011; Nutman *et al.*, 2011; Wang *et al.*, 2011, 2012, 2013), hot
754 spots driven by mantle plumes (e.g., Zhao *et al.*, 2001, 2005, 2012; Yang *et al.*, 2008; Zhai &
755 Santosh, 2011), continental rift environments (e.g., Sandiford & Powell, 1986) and continental
756 collisional belts (e.g., Niu *et al.*, 2013; Laurent *et al.*, 2014; Song *et al.*, 2014, 2015).

757 As discussed above, the Neoarchean TTG granitoids in the Xingcheng region have no
758 obvious geochemical signatures of enhanced melt-peridotite interaction, such as elevated MgO
759 contents and $Mg^{\#}$ values, Cr and Ni concentrations, which should be expected if these TTG
760 granitoids were produced through partial melting of subducting/subducted oceanic crust or
761 oceanic plateau materials (Bédard, 2006; Moyen & Martin, 2012; Moyen & van Hunen, 2012;

762 Bédard *et al.*, 2013; Martin *et al*., 2014; Sizova *et al*., 2015). However, the Neoarchean TTG
763 and potassic granitoids are the reworking products of Mesoarchean crustal materials instead of
764 juvenile addition to the crust from the mantle as implied by their bulk rock Nd and zircon Hf
765 isotopic compositions. Their Mesoarchean source rocks include enriched mafic rocks and
766 already emplaced felsic TTGs, thus they cannot be generated in subduction-related settings
767 (continental or island arcs, thickened arc systems and accretionary orogens) where mainly
768 juvenile mafic rocks act as source rocks (Bédard, 2006; Nagel *et al*., 2012; Bédard *et al.*, 2013;
769 Martin *et al*., 2014). If these TTGs were formed above hot spots driven by mantle plumes, i.e.,
770 melting at the base of a thick oceanic plateau crust heated by upwelling mantle plume (Smithies
771 *et al*., 2009), the resulting TTG rocks would be emplaced in a sequence of mantle-plume related
772 ultramafic to mafic rocks including komatiites, continental flood basalts, and deep plumbing
773 systems of dyke swarms and layered intrusions (Ernst *et al*., 2008). But no such 2.6-2.5 Ga
774 mantle plume-related magmatism has been recognized in the study area, nor global record of
775 mantle plume activity at the end of Archean (e.g., Ernst & Bleeker, 2010). Therefore, a mantle
776 plume model may be inappropriate to account for the generation of the Neoarchean TTG and
777 potassic granitoids in the Xingcheng region.

778 Bédard *et al*. (2013) proposed a model of cratonic drift in response to mantle convection
779 currents and the resulting aggregation of Archean cratons and oceanic plateaus. The accretion
780 between terranes led to thickening and delamination of mafic crust accompanied by the
781 ascending hot mantle, resulting in the coeval basalt and TTG magmas. This scenario is highly
782 unlikely for the Neoarchean TTG granitoids in the Xingcheng region as there is no coeval
783 Neoarchean basaltic magmas. Furthermore, most of the TTG granitoids in the Xingcheng region

784 formed at the medium pressure along a geotherm (15-20 °C/km; Moyen & Martin, 2012), which
785 is too low for a plateau setting but also too hot for a subduction situation even considering the
786 possibility that Archean subduction zones may be hotter. A continental rift environment is also
787 inappropriate because of lacking alkali intrusive rocks expected to be associated with rifting
788 (Zhao *et al*., 2001). Therefore, a setting of continental collision is more likely to produce the
789 Neoarchean TTG and potassic granitoids in the Xingcheng region.

790 As shown in Fig 1b, the Precambrian basement of the Eastern Block of the NCC is
791 composed of two major kinds of terranes: the high-grade metamorphic terrane and the granitic
792 terrane with no or low-grade metamorphism. The high-grade metamorphic terrane contains
793 tonalite, trandjhemite, charnockite and supracrustal rocks (ultramafic to mafic igneous rocks
794 and sedimentary rocks with BIF), with diverse protoliths and varying ages of 3.8 to 2.6 Ga (e.g.,
795 Nutman *et al.*, 2011; Zhai & Santosh, 2011), but all experienced granulite-facies metamorphism
796 at ~ 2.6-2.5 Ga (Zhao *et al*. 2001, 2005). The contemporaneous high-grade metamorphism and
797 plutonic magmatism indicate an intensive tectono-thermal event in the Late Neoarchean (2.6-
798 2.5 Ga) throughout the NCC; this event is most likely an orogenic movement because the
799 Neoarchean is an important period for the amalgamation of micro-continental blocks and
800 cratonization of the eastern NCC and the Xingcheng region lies between micro continental
801 blocks with ca. 3.8 Ga old crust nuclei (Fig 1b; Caozhuang and Anshan; Zhai & Santosh, 2011).
802 Recent reports of Neoarchean high-K calc-alkaline rocks in Western Liaoning (e.g., Wang *et*
803 *al.*, 2012, 2013) also favor this possibility.

804 As mentioned above, the Neoarchean granitoids in the eastern NCC varies from sodic-to-
805 potassic TTG granitoids, diorite-granodiorites, monzogranites to potassic-rich, peraluminous

806 granites (Yang *et al.*, 2008; this study). This rock assemblage is comparable to magmatism in
807 Phanerozoic continental collisional belts, which encompasses a series of adakitic, I-, S- and A-
808 type granites and other igneous rocks and shows large compositional variation (e.g., Himalaya,
809 North Qaidam and Caledonian orogens; Chung *et al.*, 2003; Niu *et al.*, 2013; Laurent *et al.*,
810 2014; Song *et al.*, 2014, 2015). The absence of S-type granites in the Neoarchean granitoids on
811 the eastern NCC may reflect that abundant sediments had not been developed till then. The
812 Neoarchean TTG granitoids in the Xingcheng region were generated through partial melting of
813 Mesoarchean enriched mafic crustal sources at different depth levels (up to 12 kbar or 42 km)
814 coupled with low-pressure crystal fractionation, which requires significant crustal thickening
815 through micro-continental collision (e.g., Nutman & Friend, 2007). The potassic granites, with
816 their intrusive contact with the TTG granitoids and younger age, represent the last pulse of the
817 Archean magmatism in the Xingcheng region and most likely formed by re-melting of
818 Mesoarchean TTGs or low-degree partial melting of Mesoarchean enriched mafic crustal
819 materials in an extensional or non-compressional environment, i.e., the post-orogenic or post-
820 collisional stage. These potassic granites can act as a marker for the end of an orogenic cycle
821 and final stabilization of the Archean proto-crust (Zhou *et al.*, 2011; Zhang *et al.*, 2012). The
822 melting of the Mesoarchean mafic crust was triggered by melts from the upwelling mantle,
823 which also modified the compositions of these melts by different degrees. The large variation
824 of the initial zircon Hf isotopic compositions of the Neoarchean TTG and potassic granitoids in
825 the Xingcheng region is also observed when a convergent (i.e., subduction) environment turns
826 into continental collision (Hawkesworth *et al.*, 2010; Laurent *et al.*, 2014), which is consistent
827 with an increase in reworking processes associated with crustal thickening during collision and

828 melting of the mantle sources. Numerical modeling suggested that Precambrian continental
829 collisional belts are characterized by different tectonic styles compared with modern continental
830 collisional belts as they were formed over a hotter mantle and remained mechanically weak
831 (Sizova, 2014). Thus shallow slab-break-off often took place, limiting the occurrence of
832 ultrahigh-pressure metamorphic complexes within the Precambrian continental orogenic belts
833 and allowing for frequent upwelling and subsequent melting of mantle (Moyen & van Hunen,
834 2012; Sizova, 2014). In fact, we cannot precisely constrain the details and configuration of the
835 proposed continental collisional belt for the generation of the Neoarchean TTG and potassic
836 granitoids in the Xingcheng region based the available data. It should share some similarities
837 with modern continental collisional belts in certain aspects and could be accommodated by
838 different orogenic styles, such as retreating or advancing plate boundaries followed by collision,
839 and evolve through different scenarios (e.g., slab retreat and break-off; Laurent *et al.*, 2014).

840 Together with the concurrent high-grade metamorphism widespread in the NCC, we
841 conclude that the Neoarchean granitoids in the Xingcheng region were formed through an
842 orogenic process from micro-continental collision to post-collisional extension at the late
843 Neoarchean. The micro-continents formed during Mesoarchean and at the end of Archean
844 began to accrete and amalgamate, leading to significant crustal thickening while also causing
845 granulite-facies metamorphism and partial melting of Mesoarchean enriched mafic crustal
846 materials at varying depths caused by heating from mantle-derived mafic magmas and
847 fractional crystllization. These micro-continental blocks have been intensively overprinted by
848 the 2.6-2.5 Ga orogenic event and are difficult to define, as some ~ 3.8 Ga crustal remnants
849 have been identified in some areas of the NCC. After collision, the amalgamated micro-

continental blocks underwent extension. As a result, the mafic proto-crust experienced low-degree partial melting and the Mesoarchen TTGs may have also re-melted, generating the potassic granites.

CONCLUSIONS

The Neoarchean crust in the Xingcheng region are made up of TTG granitoids and potassic granites. The TTG granitoids with MMEs formed through partial melting of Mesoarchean enriched mafic crustal sources at varying depth levels with low-pressure fractional crystallization in a collisional environment in 2595-2558 Ma. The Taili gneissic were the products of low-pressure melting of Mesoarchean enriched mafic crust with Neoarchean juvenile mantle-derived mafic melts. Two kinds of potassic granites were produced by (a) low-degree partial melting of enriched mafic crustal sources at 2540 Ma, and (b) re-melting of Mesoarchean TTGs in response to post-collisional extension at 2520 Ma. Upwelling of Neoarchean mantle-derived mafic magmas triggered the partial melting of their source rocks and modified their compositions by different degrees.

The rock assemblages in the Suizhong granitic terrane resemble those of Phanerozoic orogens and record the evolution from collision of micro-continental blocks to post-collisional extension.

The major crustal growth in the eastern NCC took place during the Neoarchean. A proto-type upper continental crust of the NCC, which made at least 70-80 % of the compositions of the present-day upper continental crust, might have been developed at the end of the Archean by mixing of TTG and potassic granitoids.

ACKNOWLEDGEMENTS

The authors are grateful to Jean-François Moyen, Tracy Rushmer and an anonymous reviewer for their detailed and constructive peer-review comments which greatly improved the quality of this manuscript. Editorial handling by Simon Turner is also gratefully acknowledged. The authors wish to thank W.G. Liu and W.P. Zhu for the help during Nd isotope analyses. This study was supported by the National Natural Science Foundation of China (grants 41430207, 41372060, 41121062 and 41130314).

REFERENCES

Adam, J., Rushmer, T., O'Neil, J., Francis, D. (2012). Hadean greenstones from the Nuvvuagittuq fold belt and the origin of the Earth's early continental crust. *Geology* **40**, 363-366.

Andersen, T. (2002). Correction of common lead in U–Pb analyses that do not report 204Pb. *Chemical Geology* **192**, 59-79.

Bédard, J. H. (2006). A catalytic delamination-driven model for coupled genesis of Archaean crust and sub-continental lithospheric mantle. *Geochimica et Cosmochimica Acta* **70**, 1188-1214.

Bédard, J. H., Harris, L. B., Thurston, P. C. (2013). The hunting of the snArc. *Precambrian Research* **229**, 20-48.

Bai, X., Liu, S., Guo, R., Wang, W. (2016). A Neoarchean arc–back-arc system in Eastern Hebei, North China Craton: Constraints from zircon U–Pb–Hf isotopes and geochemistry of dioritic–tonalitic–trondhjemitic–granodioritic (DTTG) gneisses and felsic paragneisses.

892 *Precambrian Research* **273**, 90-111.
893 Barker, F. (1979). Trondhjemite: definition, environment and hypotheses of origin. In: Barker,
894 F. (ed.) *Trondhjemites, Dacites, and Related Rocks*. Amsterdam: Elsevier, 1-12.
895 Belousova, E. A., Griffin, W. L., O'Reilly, S. Y. (2006). Zircon Crystal Morphology, Trace
896 Element Signatures and Hf Isotope Composition as a Tool for Petrogenetic Modelling:
897 Examples From Eastern Australian Granitoids. *Journal of Petrology* **47**, 329-353.
898 Black, L. P., Kamo, S. L., Allen, C. M., Aleinikoff, J. N., Davis, D. W., Korsch, R. J., Foudoulis,
899 C. (2003). TEMORA 1: a new zircon standard for Phanerozoic U–Pb geochronology.
900 *Chemical Geology* **200**, 155-170.
901 Bleeker, W. (2003). The late Archean record: a puzzle in ca. 35 pieces. *Lithos* **71**, 99-134.
902 Castillo, P. R. (2012). Adakite petrogenesis. *Lithos* **134–135**, 304-316.
903 Castro, A. (2003). The source of granites: inferences from the Lewisian complex. *Scottish*
904 *Journal of Geology* **40**, 49-66.
905 Champion, D. C. & Smithies, R. H. (2007). Chapter 4.3 Geochemistry of Paleoarchean Granites
906 of the East Pilbara Terrane, Pilbara Craton, Western Australia: Implications for Early
907 Archean Crustal Growth. In: Martin J. van Kranendonk, R. H. S. & Vickie, C. B. (eds.)
908 *Developments in Precambrian Geology*: Elsevier, 369-409.
909 Chappel, B. W., White, A. J. R., Wyborn, D. (1987). The Importance of Residual Source
910 Material (Restite) in Granite Petrogenesis. *Journal of Petrology* **28**, 1111-1138.
911 Chappell, B. W. (1999). Aluminium saturation in I- and S-type granites and the characterization
912 of fractionated haplogranites. *Lithos* **46**, 535-551.
913 Chen, B., Jahn, B.-m., Wei, C. (2002). Petrogenesis of Mesozoic granitoids in the Dabie UHP

914 complex, Central China: trace element and Nd-Sr isotope evidence. *Lithos* **60**, 67-88.
915 Chen, S., Niu, Y., Sun, W., Zhang, Y., Li, J., Guo, P., Sun, P. (2015). On the origin of mafic
916 magmatic enclaves (MMEs) in syn-collisional granitoids: evidence from the Baojishan
917 pluton in the North Qilian Orogen, China. *Mineralogy and Petrology* **109**, 577-596.
918 Chen, S., Y.L. Niu, J.Y. Li, W.L. Sun, Y. Zhang, Y. Hu & F.L. Shao, 2016. Syncollisional
919 adakitic granodiorites formed by fractional crystallization: insights from their enclosed
920 mafic magmatiuc enclaves (MMEs) in the Qumushan pluton, North Qilian Orogen at the
921 northern margin of the Tibetan Plateau. *Lithos* **248/251**, 455-468.
922 Chen, Y., Song, S., Niu, Y., Wei, C. (2014). Melting of continental crust during subduction
923 initiation: A case study from the Chaidanuo peraluminous granite in the North Qilian suture
924 zone. *Geochimica et Cosmochimica Acta* **132**, 311-336.
925 Chung, S. L., Liu, D. Y., Ji, J. Q., Chu, M. F., Lee, H. Y., Wen, D. J., Lo, C. H., Lee, T. Y., Qian,
926 Q., Zhang, Q. (2003). Adakites from continental collision zones: Melting of thickened
927 lower crust beneath southern Tibet. *Geology* **31**, 1021-1024.
928 Compston, W., Zhong, F. D., Foster, J. J., Collerson, K. D., Bai, J., Sun, D. C. (1983). Rubidium-
929 strontium geochronology of Precambrian rocks from the Yenshan region, North China.
930 *Precambrian Research* **22**, 175-202.
931 Condie, K. C. (1993). Chemical composition and evolution of the upper continental crust:
932 Contrasting results from surface samples and shales. *Chemical Geology* **104**, 1-37.
933 Condie, K. C. (2005a). High field strength element ratios in Archean basalts: a window to
934 evolving sources of mantle plumes? *Lithos* **79**, 491-504.
935 Condie, K. C. (2005b). TTGs and adakites: are they both slab melts? *Lithos* **80**, 33-44.

936 Condie, K. C. (2008). Did the character of subduction change at the end of the Archean?
937 Constraints from convergent-margin granitoids. *Geology* **36**, 611-614.
938 Condie, K.C. (2014) How to Make a Continent: Thirty-fiveYears of TTG Research. Y. Dilek,
939 H. Furnes (eds.) *Evolution of Archean Crust and Early Life, Modern Approaches in Solid*
940 *Earth Sciences* **7**, 179-193. DOI 10.1007/978-94-007-7615-9_7, © Springer Science-
941 Business Media Dordrecht 2014
942 Condie, K. C. & Aster, R. C. (2010). Episodic zircon age spectra of orogenic granitoids: The
943 supercontinent connection and continental growth. *Precambrian Research* **180**, 227-236.
944 Condie, K. C., Bickford, M. E., Aster, R. C., Belousova, E., Scholl, D. W. (2011). Episodic
945 zircon ages, Hf isotopic composition, and the preservation rate of continental crust.
946 *Geological Society of America Bulletin* **123**, 951-957.
947 Condie, K. C. & Kröner, A. (2013). The building blocks of continental crust: Evidence for a
948 major change in the tectonic setting of continental growth at the end of the Archean.
949 *Gondwana Research* **23**, 394-402.
950 Defant, M. J. & Drummond, M. S. (1990). Derivation of some modern arc magmas by melting
951 of young subducted lithosphere. *Nature* **347**, 662-665.
952 Ernst, R. & Bleeker, W. (2010). Large igneous provinces (LIPs), giant dyke swarms, and mantle
953 plumes: significance for breakup events within Canada and adjacent regions from 2.5 Ga
954 to the Present. *Canadian Journal of Earth Sciences* **47**, 695-739.
955 Ernst, R. E., Wingate, M. T. D., Buchan, K. L., Li, Z. X. (2008). Global record of 1600–
956 700 Ma Large Igneous Provinces (LIPs): Implications for the reconstruction of the
957 proposed Nuna (Columbia) and Rodinia supercontinents. *Precambrian Research* **160**, 159-

178.

Foley, S., Tiepolo, M., Vannucci, R. (2002). Growth of early continental crust controlled by melting of amphibolite in subduction zones. *Nature* **417**, 837-840.

Frost, C. D., Frost, B. R., Chamberlain, K. R., Hulsebosch, T. P. (1998). The Late Archean history of the Wyoming province as recorded by granitic magmatism in the Wind River Range, Wyoming. *Precambrian Research* **89**, 145-173.

Geng, Y. S., Shen, Q. H., Ren, L. D. (2010). Late Neoarchean to Early Paleoproterozoic magmatic events and tectonothermal systems in the North China Craton. *Acta Petrologica Sinica* **26**, 1945-1966. (In Chinese with English abstract)

Guo, J. H., O'Brien, P. J., Zhai, M. (2002). High-pressure granulites in the Sanggan area, North China craton: metamorphic evolution, P–T paths and geotectonic significance. *Journal of Metamorphic Geology* **20**, 741-756.

Griffin, W. L., Wang, X., Jackson, S. E., Pearson, N. J., O'Reilly, S. Y., Xu, X., Zhou, X. (2002). Zircon chemistry and magma mixing, SE China: In-situ analysis of Hf isotopes, Tonglu and Pingtan igneous complexes. *Lithos* **61**, 237-269.

Hawkesworth, C. J., Dhuime, B., Pietranik, A. B., Cawood, P. A., Kemp, A. I. S., Storey, C. D. (2010). The generation and evolution of the continental crust. *Journal of the Geological Society* **167**, 229-248.

Hoffmann, J. E., Nagel, T. J., Münker, C., Næraa, T., Rosing, M. T. (2014). Constraining the process of Eoarchean TTG formation in the Itsaq Gneiss Complex, southern West Greenland. *Earth and Planetary Science Letters* **388**, 374-386.

Holden, P., Halliday, A. N., Stephens, W. E. (1987). Neodymium and strontium isotope content

of microdiorite enclaves points to mantle input to granitoid production. *Nature* **330**, 53-56.

Hollings, P. & Kerrich, R. (2006). Light rare earth element depleted to enriched basaltic flows from 2.8 to 2.7 Ga greenstone belts of the Uchi Subprovince, Ontario, Canada. *Chemical Geology* **227**, 133-153.

Hou, K. J., Li, Y. H., Zou, T. R., Qu, X. M., Shi, Y. R., Xie, G. Q. (2007). Laser ablation-MC-ICP-MS technique for Hf isotope microanalysis of zircon and its geological applications. *Acta Petrologica Sinica* **23 (10)**, 2595-2604. (In Chinese with English abstract)

Huang, H., Niu, Y., Nowell, G., Zhao, Z., Yu, X., Zhu, D.-C., Mo, X., Ding, S. (2014). Geochemical constraints on the petrogenesis of granitoids in the East Kunlun Orogenic belt, northern Tibetan Plateau: Implications for continental crust growth through syn-collisional felsic magmatism. *Chemical Geology* **370**, 1-18.

Jahn, B.-M., Auvray, B., Blais, S., Capdevila, R., Cornichet, J., Vidal, F., Hameurt, J. (1980). Trace element geochemistry and petrogenesis of Finnish greenstone belts. *Journal of Petrology* **21**, 201-244.

Jahn, B.-M. & Ernst, W. G. (1990). Late Archean Sm-Nd isochron age for Mafic-ultramafic supracrustal amphibolites from the Northeastern Sino-Korean Craton, China. *Precambrian Research* **46**, 295-306.

Jahn, B. M., Glikson, A. Y., Peucat, J. J., Hickman, A. H. (1981). REE geochemistry and isotopic data of Archean silicic volcanics and granitoids from the Pilbara Block, Western Australia: implications for the early crustal evolution. *Geochimica et Cosmochimica Acta* **45**, 1633-1652.

Jiang, N., Guo, J. H., Zhai, M. G., Zhang, S. Q. (2010). ~2.7 Ga crust growth in the North China

1002 craton. *Precambrian Research* **179**, 37-49.
1003 Jayananda, M., Chardon, D., Peucat, J. J., Capdevila, R. (2006). 2.61Ga potassic granites and
1004 crustal reworking in the western Dharwar craton, southern India: Tectonic, geochronologic
1005 and geochemical constraints. *Precambrian Research* **150**, 1-26.
1006 Kröner, A., Cui, W.-Y., Wang, S.-Q., Wang, C.-Q., Nemchin, A. A. (1998). Single zircon ages
1007 from high-grade rocks of the Jianping Complex, Liaoning Province, NE China. *Journal of*
1008 *Asian Earth Sciences* **16**, 519-532.
1009 Laurent, O., Martin, H., Moyen, J. F., Doucelance, R. (2014). The diversity and evolution of
1010 late-Archean granitoids: Evidence for the onset of "modern-style" plate tectonics between
1011 3.0 and 2.50 Ga. *Lithos* **205**, 208-235.
1012 Li, S. & Zhao, G. (2007). SHRIMP U–Pb zircon geochronology of the Liaoji granitoids:
1013 Constraints on the evolution of the Paleoproterozoic Jiao-Liao-Ji belt in the Eastern Block
1014 of the North China Craton. *Precambrian Research* **158**, 1-16.
1015 Liu, D. Y., Nutman, A. P., Compston, W., Wu, J. S., Shen, Q. H. (1992). Remnants of ≥3800
1016 Ma crust in the Chinese part of the Sino-Korean craton. *Geology* **20**, 339-342.
1017 Liu, J., Liu, F., Ding, Z., Liu, C., Yang, H., Liu, P., Wang, F., Meng, E. (2013a). The growth,
1018 reworking and metamorphism of early Precambrian crust in the Jiaobei terrane, the North
1019 China Craton: Constraints from U–Th–Pb and Lu–Hf isotopic systematics, and REE
1020 concentrations of zircon from Archean granitoid gneisses. *Precambrian Research* **224**,
1021 287-303.
1022 Liu, S. W., Santosh, M., Wang, W., Bai, X., Yang, P. T. (2011). Zircon U–Pb chronology of the
1023 Jianping Complex: Implications for the Precambrian crustal evolution history of the

1024 northern margin of North China Craton. *Gondwana Research* **20**, 48-63.
1025 Liu, S., Wan, Y., Sun, H., Nutman, A. P., Xie, H., Dong, C., Ma, M., Liu, D., Jahn, B.-m. (2013b).
1026 Paleo- to Eoarchean crustal evolution in eastern Hebei, North China Craton: New evidence
1027 from SHRIMP U–Pb dating and in-situ Hf isotopic study of detrital zircons from
1028 paragneisses. *Journal of Asian Earth Sciences* **78**, 4-17.
1029 Liu, S. W., Wang, W., Bai, X., Zhang, F., Yang, P. T. (2010). Geological events of Early
1030 Precambrian complex in North Chaoyang Area, Liaoning Province. *Acta Petrologica*
1031 *Sinica* **26**, 1993-2004. (In Chinese with English abstract)
1032 Ludwig, K. R. (2003). *User's manual for Isoplot 3.0: a Geochronological Toolkit for Microsoft*
1033 *Excel*: Berkeley Geochronology Centre, Special Publication.
1034 Macpherson, C. G., Dreher, S. T., Thirlwall, M. F. (2006). Adakites without slab melting: High
1035 pressure differentiation of island arc magma, Mindanao, the Philippines. *Earth and*
1036 *Planetary Science Letters* **243**, 581-593.
1037 Martin, H. (1999). Adakitic magmas: modern analogues of Archaean granitoids. *Lithos* **46**, 411-
1038 429.
1039 Martin, H., Moyen, J.-F., Guitreau, M., Blichert-Toft, J., Le Pennec, J.-L. (2014). Why
1040 Archaean TTG cannot be generated by MORB melting in subduction zones. *Lithos* **198–**
1041 **199**, 1-13.
1042 Martin, H., Smithies, R. H., Rapp, R., Moyen, J. F., Champion, D. (2005). An overview of
1043 adakite, tonalite-trondhjemite-granodiorite (TTG), and sanukitoid: relationships and some
1044 implications for crustal evolution. *Lithos* **79**, 1-24.
1045 Miller, J., Moyen, J.-F., Benn, K. (2008). The 2.74-2.66 Ga Kenogamissi complex (Abitibi):

1046 Evolving sources of plutons mirroring geodynamics. *Geochimica et Cosmochimica Acta*
1047 *Supplement* **72**, 629.
1048 Morel, M. L. A., Nebel, O., Nebel-Jacobsen, Y. J., Miller, J. S., Vroon, P. Z. (2008). Hafnium
1049 isotope characterization of the GJ-1 zircon reference material by solution and laser-ablation
1050 MC-ICPMS. *Chemical Geology* **255**, 231-235.
1051 Moyen, J.-F. (2011). The composite Archaean grey gneisses: Petrological significance, and
1052 evidence for a non-unique tectonic setting for Archaean crustal growth. *Lithos* **123**, 21-36.
1053 Moyen, J.-F., Champion, D., Smithies, R. H. (2010). The geochemistry of Archaean
1054 plagioclase-rich granites as a marker of source enrichment and depth of melting.
1055 *Geological Society of America Special Papers* **472**, 35-50.
1056 Moyen, J.-F. & Martin, H. (2012). Forty years of TTG research. *Lithos* **148**, 312-336.
1057 Moyen, J.-F., Martin, H., Jayananda, M. (2001). Multi-element geochemical modelling of
1058 crust–mantle interactions during late-Archaean crustal growth: the Closepet granite (South
1059 India). *Precambrian Research* **112**, 87-105.
1060 Moyen, J. F., Martin, H., Jayananda, M., Auvray, B. (2003). Late Archaean granites: a typology
1061 based on the Dharwar Craton (India). *Precambrian Research* **127**, 103-123.
1062 Moyen, J.-F., Stevens, G., Kisters, A. F. M., Belcher, R. W. (2007). Chapter 5.6 TTG Plutons of
1063 the Barberton Granitoid-Greenstone Terrain, South Africa. In: Martin J. van Kranendonk,
1064 R. H. S. & Vickie, C. B. (eds.) *Developments in Precambrian Geology*: Elsevier, 607-667.
1065 Moyen, J.-F. & van Hunen, J. (2012). Short-term episodicity of Archaean plate tectonics.
1066 *Geology* **40**, 451-454.
1067 Nagel, T. J., Hoffmann, J. E., Münker, C. (2012). Generation of Eoarchean tonalite-

trondhjemite-granodiorite series from thickened mafic arc crust. *Geology* **40**, 375-378.

Niu, Y., Zhao, Z., Zhu, D.-C., Mo, X. (2013). Continental collision zones are primary sites for net continental crust growth — A testable hypothesis. *Earth-Science Reviews* **127**, 96-110.

Nutman, A. P. & Friend, C. R. L. (2007). Adjacent terranes with ca. 2715 and 2650 Ma high-pressure metamorphic assemblages in the Nuuk region of the North Atlantic Craton, southern West Greenland: Complexities of Neoarchaean collisional orogeny. *Precambrian Research* **155**, 159-203.

Nutman, A. P., Wan, Y., Du, L., Friend, C. R. L., Dong, C., Xie, H., Wang, W., Sun, H., Liu, D. (2011). Multistage late Neoarchaean crustal evolution of the North China Craton, eastern Hebei. *Precambrian Research* **189**, 43-65.

Patiño Douce, A. E. (2005). Vapor-Absent Melting of Tonalite at 15–32 kbar. *Journal of Petrology* **46**, 275-290.

PATIÑO DOUCE, A. E. & BEARD, J. S. (1995). Dehydration-melting of Biotite Gneiss and Quartz Amphibolite from 3 to 15 kbar. *Journal of Petrology* **36**, 707-738.

Qian, J., Wei, C., Zhou, X., Zhang, Y. (2013). Metamorphic P–T paths and New Zircon U–Pb age data for garnet–mica schist from the Wutai Group, North China Craton. *Precambrian Research* **233**, 282-296.

Qian, Q. & Hermann, J. (2013). Partial melting of lower crust at 10–15 kbar: constraints on adakite and TTG formation. *Contributions to Mineralogy and Petrology*, **165**, 1195-1224

Rapp, R. P., Shimizu, N., Norman, M. D. (2003). Growth of early continental crust by partial melting of eclogite. *Nature* **425**, 605-609.

Rapp, R. P., Shimizu, N., Norman, M. D., Applegate, G. S. (1999). Reaction between slab-

derived melts and peridotite in the mantle wedge: experimental constraints at 3.8 GPa. *Chemical Geology* **160**, 335-356.

Rapp, R. P. & Watson, E. B. (1995). Dehydration Melting of Metabasalt at 8–32 kbar: Implications for Continental Growth and Crust-Mantle Recycling. *Journal of Petrology* **36**, 891-931.

Rapp, R. P., Watson, E. B., Miller, C. F. (1991). Partial melting of amphibolite/eclogite and the origin of Archean trondhjemites and tonalites. *Precambrian Research* **51**, 1-25.

Rapp, R. P., Xiao, L., Shimizu, N. (2002). Experimental contraints on the origin of potassium-rich adakties in eastern China. *Acta Petrologica Sinica*, 293-302.

Rudnick R. L. & Gao S. (2003) Composition of the continental crust. In: R. L. Rudnick (ed.) *The Crust*, vol. 3. Elsevier, pp. 1-64.

Samsonov, A. V., Bogina, M. M., Bibikova, E. V., Petrova, A. Y., Shchipansky, A. A. (2005). The relationship between adakitic, calc-alkaline volcanic rocks and TTGs: implications for the tectonic setting of the Karelian greenstone belts, Baltic Shield. *Lithos* **79**, 83-106.

Sandiford, M. & Powell, R. (1986). Deep crustal metamorphism during continental extension: modern and ancient examples. *Earth and Planetary Science Letters* **79**, 151-158.

Santosh, M., Tsunogae, T., Li, J. H., Liu, S. J. (2007a). Discovery of sapphirine-bearing Mg–Al granulites in the North China Craton: Implications for Paleoproterozoic ultrahigh temperature metamorphism. *Gondwana Research* **11**, 263-285.

Santosh, M., Wilde, S. A., Li, J. H. (2007b). Timing of Paleoproterozoic ultrahigh-temperature metamorphism in the North China Craton: Evidence from SHRIMP U–Pb zircon geochronology. *Precambrian Research* **159**, 178-196.

1112 Sen, C. & Dunn, T. (1994). Dehydration melting of a basaltic composition amphibolite at 1.5
1113 and 2.0 GPa: implications for the origin of adakites. *Contributions to Mineralogy and*
1114 *Petrology* **117**, 394-409.
1115 Shi, Y. R., Wilde, S. A., Zhao, X. T., Ma, Y. S., Du, L. L., Liu, D. Y. (2012). Late Neoarchean
1116 magmatic and subsequent metamorphic events in the northern North China Craton:
1117 SHRIMP zircon dating and Hf isotopes of Archean rocks from Yunmengshan Geopark,
1118 Miyun, Beijing. *Gondwana Research* **21**, 785-800.
1119 Sisson, T., Ratajeski, K., Hankins, W., Glazner, A. (2005). Voluminous granitic magmas from
1120 common basaltic sources. *Contributions to Mineralogy and Petrology* **148**, 635-661.
1121 Sizova, E., Gerya, T., Brown, M. (2014). Contrasting styles of Phanerozoic and Precambrian
1122 continental collision. *Gondwana Research* **25**, 522-545.
1123 Sizova, E., Gerya, T., Stüwe, K., Brown, M. (2015). Generation of felsic crust in the Archean:
1124 A geodynamic modeling perspective. *Precambrian Research* **271**, 198-224.
1125 Skjerlie, K. P. & Johnston, A. D. (1996). Vapour-Absent Melting from 10 to 20 kbar of Crustal
1126 Rocks that Contain Multiple Hydrous Phases: Implications for Anatexis in the Deep to Very
1127 Deep Continental Crust and Active Continental Margins. *Journal of Petrology* **37**, 661-691.
1128 Skjerlie, K. P. & Patiño Douce, A. E. (2002). The Fluid-absent Partial Melting of a Zoisite-
1129 bearing Quartz Eclogite from 1·0 to 3·2 GPa; Implications for Melting in Thickened
1130 Continental Crust and for Subduction-zone Processes. *Journal of Petrology* **43**, 291-314.
1131 Smithies, R. H. (2000). The Archaean tonalite-trondhjemite-granodiorite (TTG) series is not an
1132 analogue of Cenozoic adakite. *Earth and Planetary Science Letters* **182**, 115-125.
1133 Smithies, R.H., Champion, D.C., Van Kranendonk, M.J. (2009). Formation of Paleoarchean

continental crust through infracrustal melting of enriched basalt. *Earth and Planetary Science Letters* **281**, 298-306.

Song, B., Nutman, A. P., Liu, D. Y., Wu, J. S. (1996). 3800 to 2500 Ma crustal evolution in the Anshan area of Liaoning Province, northeastern China. *Precambrian Research* **78**, 79-94.

Song, S., Niu, Y., Su, L., Wei, C., Zhang, L. (2014). Adakitic (tonalitic-trondhjemitic) magmas resulting from eclogite decompression and dehydration melting during exhumation in response to continental collision. *Geochimica et Cosmochimica Acta* **130**, 42-62.

Song, S., Wang, M., Wang, C., Niu, Y. (2015). Magmatism during continental collision, subduction, exhumation and mountain collapse in collisional orogenic belts and continental net growth: A perspective. *Science China Earth Sciences* **58**, 1284-1304.

Song, S. G., Niu, Y. L., Wei, C. J., Ji, J. Q., Su, L. (2010a). Metamorphism, anatexis, zircon ages and tectonic evolution of the Gongshan block in the northern Indochina continent—An eastern extension of the Lhasa Block. *Lithos* **120**, 327-346.

Song, S. G., Su, L., Li, X. H., Zhang, G. B., Niu, Y. L., Zhang, L. F. (2010b). Tracing the 850-Ma continental flood basalts from a piece of subducted continental crust in the North Qaidam UHPM belt, NW China. *Precambrian Research* **183**, 805-816.

Sun, J. F., Yang, J. H., Wu, F. Y., Wilde, S. A. (2012). Precambrian crustal evolution of the eastern North China Craton as revealed by U–Pb ages and Hf isotopes of detrital zircons from the Proterozoic Jing'eryu Formation. *Precambrian Research* **200–203**, 184-208.

Sun, S. S. & McDonough, W. F. (1989). Chemical and isotopic systematics of oceanic basalts: implications for mantle composition and processes. *Geological Society, London, Special Publications* **42**, 313-345.

1156 Sylvester, P. J. (1994). Archaean granite plutons. In: Condie, K. C. (ed.) *Archaean Crustal*
1157 *Evolution*. Netherlands: Elsevier Science,, 261-314.
1158 Tam, P. Y., Zhao, G., Liu, F., Zhou, X., Sun, M., Li, S. (2011). Timing of metamorphism in the
1159 Paleoproterozoic Jiao-Liao-Ji Belt: New SHRIMP U–Pb zircon dating of granulites,
1160 gneisses and marbles of the Jiaobei massif in the North China Craton. *Gondwana Research*
1161 **19**, 150-162.
1162 van Hunen, J. & Moyen, J.-F. (2012). Archean Subduction: Fact or Fiction? *Annual Review of*
1163 *Earth and Planetary Sciences* **40**, 195-219.
1164 Vernon, R. H. (1984). Microgranitoid enclaves in granites[mdash]globules of hybrid magma
1165 quenched in a plutonic environment. *Nature* **309**, 438-439.
1166 Wall, V. J., Clemens, J. D., Clarke, D. B. (1987). Models for granitoid evolution and source
1167 compositions. *Journal of Geology* **95**, 731-749.
1168 Wan, Y., Liu, D., Wang, S., Dong, C., Yang, E., Wang, W., Zhou, H., Ning, Z., Du, L., Yin, X.,
1169 Xie, H., Ma, M. (2010). Juvenile magmatism and crustal recycling at the end of the
1170 Neoarchean in Western Shandong Province, North China Craton: Evidence from SHRIMP
1171 zircon dating. *American Journal of Science* **310**, 1503-1552.
1172 Wan, Y., Liu, D., Wang, W., Song, T., Kröner, A., Dong, C., Zhou, H., Yin, X. (2011).
1173 Provenance of Meso- to Neoproterozoic cover sediments at the Ming Tombs, Beijing,
1174 North China Craton: An integrated study of U–Pb dating and Hf isotopic measurement of
1175 detrital zircons and whole-rock geochemistry. *Gondwana Research* **20**, 219-242.
1176 Wan, Y. S., Liu, D. Y., Song, B., Wu, J. S., Yang, C. H., Zhang, Z. Q., Geng, Y. S. (2005).
1177 Geochemical and Nd isotopic compositions of 3.8 Ga meta-quartz dioritic and

1178 trondhjemitic rocks from the Anshan area and their geological significance. *Journal of*
1179 *Asian Earth Sciences* **24**, 563-575.
1180 Wan, Y., Liu, D., Yin, X., Simon A, W., Xie, L., Yang, Y., Zhou, H., Wu, J. (2007). SHRIMP
1181 geochronology and Hf isotope composition of zircons from the Tiejiashan granite and
1182 supracrustal rocks in the Anshan area, Liaoning Province. *Acta Petrologica Sinica* **23**, 241-
1183 252. (In Chinese with English abastract)
1184 Wan, Y., Ma, M., Dong, C., Xie, H., Xie, S., Ren, P., Liu, D. (2015). Widespread late
1185 Neoarchean reworking of Meso- to Paleoarchean continental crust in the Anshan-Benxi
1186 area, North China Craton, as documented by U-Pb-Nd-Hf-O isotopes. *American Journal*
1187 *of Science* **315**, 620-670.
1188 Wang, A. D. & Liu, Y. C. (2012). Neoarchean (2.5–2.8 Ga) crustal growth of the North China
1189 Craton revealed by zircon Hf isotope: A synthesis. *Geoscience Frontiers* **3**, 147-173.
1190 Wang, C., Song, S., Niu, Y., Su, L. (2015a). Late Triassic adakitic plutons within the Archean
1191 terrane of the North China Craton: Melting of the ancient lower crust at the onset of the
1192 lithospheric destruction. *Lithos* **212-215**, 353-367.
1193 Wang, M., Song, S., Niu, Y., Su, L. (2014a). Post-collisional magmatism: Consequences of
1194 UHPM terrane exhumation and orogen collapse, N. Qaidam UHPM belt, NW China. *Lithos*
1195 **210–211**, 181-198.
1196 Wang, W., Zhai, M., Li, T., Santosh, M., Zhao, L., Wang, H. (2014b). Archean–Paleoproterozoic
1197 crustal evolution in the eastern North China Craton: Zircon U–Th–Pb and Lu–Hf evidence
1198 from the Jiaobei terrane. Precambrian Research 241, 146-160.
1199 Wang, Q., Xu, J. F., Jian, P., Bao, Z. W., Zhao, Z. H., Li, C. F., Xiong, X. L., Ma, J. L. (2006).

Petrogenesis of Adakitic Porphyries in an Extensional Tectonic Setting, Dexing, South China: Implications for the Genesis of Porphyry Copper Mineralization. *Journal of Petrology* **47**, 119-144.

Wang, W., Liu, S., Santosh, M., Bai, X., Li, Q., Yang, P., Guo, R. (2013). Zircon U–Pb–Hf isotopes and whole-rock geochemistry of granitoid gneisses in the Jianping gneissic terrane, Western Liaoning Province: Constraints on the Neoarchean crustal evolution of the North China Craton. *Precambrian Research* **224**, 184-221.

Wang, W., Liu, S., Santosh, M., Wang, G., Bai, X., Guo, R. (2015b). Neoarchean intra-oceanic arc system in the Western Liaoning Province: Implications for Early Precambrian crustal evolution in the Eastern Block of the North China Craton. *Earth-Science Reviews* **150**, 329-364.

Wang, W., Liu, S., Wilde, S. A., Li, Q., Zhang, J., Bai, X., Yang, P., Guo, R. (2012). Petrogenesis and geochronology of Precambrian granitoid gneisses in Western Liaoning Province: Constraints on Neoarchean to early Paleoproterozoic crustal evolution of the North China Craton. *Precambrian Research* **222–223**, 290-311.

Wang, W., Liu, S. W., Bai, X., Yang, P. T., Li, Q. G., Zhang, L. F. (2011). Geochemistry and zircon U–Pb–Hf isotopic systematics of the Neoarchean Yixian–Fuxin greenstone belt, northern margin of the North China Craton: Implications for petrogenesis and tectonic setting. *Gondwana Research* **20**, 64-81.

Watkins, J., Clemens, J., Treloar, P. (2007). Archaean TTGs as sources of younger granitic magmas: melting of sodic metatonalites at 0.6–1.2 GPa. *Contributions to Mineralogy and Petrology* **154**, 91-110.

1222 Wei, C., Qian, J., Zhou, X. (2014). Paleoproterozoic crustal evolution of the Hengshan–Wutai–
1223 Fuping region, North China Craton. *Geoscience Frontiers* **5**, 485-497.
1224 Whalen, J. B., Percival, J. A., McNicoll, V. J., Longstaffe, F. J. (2004). Geochemical and
1225 isotopic (Nd–O) evidence bearing on the origin of late- to post-orogenic high-K granitoid
1226 rocks in the Western Superior Province: implications for late Archean tectonomagmatic
1227 processes. *Precambrian Research* **132**, 303-326.
1228 Wiedenbeck, M., AllÉ, P., Corfu, F., Griffin, W. L., Meier, M., Oberli, F., Quadt, A. V., Roddick,
1229 J. C., Spiegel, W. (1995). Three natural zircon standards for U-Th-Pb, Lu-Hf, trace element
1230 and REE analyses. *Geostandards Newsletter* **19**, 1-23.
1231 Wu, F., Li, X., Zheng, Y., Gao, S. (2007). Lu-Hf isotopic systematics and their application in
1232 petrology. *Acta Petrologica Sinica* **23**, 185-220.
1233 Wu, F.-Y., Yang, Y.-H., Xie, L.-W., Yang, J.-H., Xu, P. (2006). Hf isotopic compositions of the
1234 standard zircons and baddeleyites used in U–Pb geochronology. *Chemical Geology* **234**,
1235 105-126.
1236 Wu, F., Yang, J., Liu, X., Li, T., Xie, L., Yang, Y. (2005a). Hf isotopes of the 3.8 Ga zircons in
1237 eastern Hebei Province, China: Implications for early crustal evolution of the North China
1238 Craton. *Chinese Science Bulletin* **50**, 2473-2480.
1239 Wu, F. Y., Zhao, G. C., Wilde, S. A., Sun, D. Y. (2005b). Nd isotopic constraints on crustal
1240 formation in the North China Craton. *Journal of Asian Earth Sciences* **24**, 523-545.
1241 Wu, M., Zhao, G., Sun, M., Li, S., Bao, Z., Tam, P. Y., Eizenhöefer, P. R., He, Y. (2014). Zircon
1242 U–Pb geochronology and Hf isotopes of major lithologies from the Jiaodong Terrane:
1243 Implications for the crustal evolution of the Eastern Block of the North China Craton.

Lithos **190-191**, 71-84.

Xiao, L. & Clemens, J. D. (2007). Origin of potassic (C-type) adakite magmas: Experimental and field constraints. *Lithos* **95**, 399-414.

Xie, S., Xie, H., Wang, S., Kröner, A., Liu, S., Zhou, H., Ma, M., Dong, C., Liu, D., Wan, Y. (2014). Ca. 2.9 Ga granitoid magmatism in eastern Shandong, North China Craton: Zircon dating, Hf-in-zircon isotopic analysis and whole-rock geochemistry. *Precambrian Research* **255**, **Part 2**, 538-562.

Yang, J., Gao, S., Chen, C., Tang, Y. Y., Yuan, H. L., Gong, H. J., Xie, S. W., Wang, J. Q. (2009). Episodic crustal growth of North China as revealed by U–Pb age and Hf isotopes of detrital zircons from modern rivers. *Geochimica et Cosmochimica Acta* **73**, 2660-2673.

Yang, J. H., Wu, F. Y., Wilde, S., Xie, L. W., Yang, Y. H., Liu, X. M. (2007). Tracing magma mixing in granite genesis: in situ U–Pb dating and Hf-isotope analysis of zircons. *Contributions to Mineralogy and Petrology* **153**, 177-190.

Yang, J. H., Wu, F. Y., Wilde, S. A., Zhao, G. C. (2008). Petrogenesis and geodynamics of Late Archean magmatism in eastern Hebei, eastern North China Craton: Geochronological, geochemical and Nd–Hf isotopic evidence. *Precambrian Research* **167**, 125-149.

Zeh, A., Gerdes, A., Barton, J. M. (2009). Archean Accretion and Crustal Evolution of the Kalahari Craton—the Zircon Age and Hf Isotope Record of Granitic Rocks from Barberton/Swaziland to the Francistown Arc. *Journal of Petrology* **50**, 933-966.

Zhai, M., Li, T. S., Peng, P., Hu, B., Liu, F., Zhang, Y. (2010). Precambrian key tectonic events and evolution of the North China craton. *Geological Society, London, Special Publications* **338**, 235-262.

1266 Zhai, M. G. & Santosh, M. (2011). The early Precambrian odyssey of the North China Craton:
1267 A synoptic overview. *Gondwana Research* **20**, 6-25.
1268 Zhang, C.-L., Li, H.-K., Santosh, M., Li, Z.-X., Zou, H.-B., Wang, H., Ye, H. (2012).
1269 Precambrian evolution and cratonization of the Tarim Block, NW China: Petrology,
1270 geochemistry, Nd-isotopes and U–Pb zircon geochronology from Archaean gabbro-TTG–
1271 potassic granite suite and Paleoproterozoic metamorphic belt. *Journal of Asian Earth*
1272 *Sciences* **47**, 5-20.
1273 Zhang, Y., Wei, C., Tian, W., Zhou, X. (2013). Reinterpretation of metamorphic age of the
1274 Hengshan Complex, North China Craton. *Chinese Science Bulletin* **58**, 4300-4307.
1275 Zhao, G. & Cawood, P. A. (2012). Precambrian geology of China. *Precambrian Research* **222-**
1276 **223**, 13-54.
1277 Zhao, G., Wilde, S. A., Cawood, P. A., Liangzhao, L. (1999). Thermal evolution of two textural
1278 types of mafic granulites in the North China Craton; evidence for both mantle plume and
1279 collisional tectonics. *Geological Magazine* **136**, 223-240.
1280 Zhao, G., Wilde, S. A., Guo, J., Cawood, P. A., Sun, M., Li, X. (2010). Single zircon grains
1281 record two Paleoproterozoic collisional events in the North China Craton. *Precambrian*
1282 *Research* **177**, 266-276.
1283 Zhao, G. C., Sun, M., Wilde, S. A., Li, S. Z. (2005). Late Archean to Paleoproterozoic evolution
1284 of the North China Craton: key issues revisited. *Precambrian Research* **136**, 177-202.
1285 Zhao, G. C., Wilde, S. A., Cawood, P. A., Lu, L. Z. (1998). Thermal Evolution of Archean
1286 Basement Rocks from the Eastern Part of the North China Craton and Its Bearing on
1287 Tectonic Setting. *International Geology Review* **40**, 706-721.

Zhao, G. C., Wilde, S. A., Cawood, P. A., Sun, M. (2001). Archean blocks and their boundaries in the North China Craton: lithological, geochemical, structural and P–T path constraints and tectonic evolution. *Precambrian Research* **107**, 45-73.

Zhou, Y.-Y., Zhao, T.-P., Wang, C. Y., Hu, G.-H. (2011). Geochronology and geochemistry of 2.5 to 2.4Ga granitic plutons from the southern margin of the North China Craton: Implications for a tectonic transition from arc to post-collisional setting. *Gondwana Research* **20**, 171-183.

FIGURE CAPTIONS

Fig 1 (a) Schematic map showing major Precambrian tectonic units of the NCC (modified after Zhao *et al.*, 2005), EH: Eastern Hebei, WL: Western Liaoning, NL-SJ: Northern Liaoning-Southern Jilin, WS: Western Shandong, ES: Eastern Shandong; (b) Simplified geological map of the northern part of the Eastern Block of the NCC; (c) Simplified geological map of the Xingcheng region; black stars indicate sampling locations.

Fig 2 Field photos of the Neoarchean TTGs and potassic granitoids in the Xingcheng region. (a) Neoarchean gneissic tonalite-granites in Taili intruded by Triassic adakitic plutons; (b) gneissic tonalites and gneissic granites in Taili, mafic sills are also shown; (c) and (d) Tonalite-trondhjemites and MMEs in Xingcheng; (e) Tonalite-trondhjemites, MMEs and syn-plutonic dykes in Xingcheng intruded by pegmatite dykes; (f) Tonalite-trondhjemites in Xingcheng intruded by potassic granites and they were both intruded by pegmatite dykes; (g) Granodiorites and MMEs in Juhuadao; (h) Potassic granites in Huludao unconformably overlain by the

Paleoproterozoic sedimentary rocks of the Changcheng formation (Pt_{2c}).

Fig 3 Cathodoluminescence (CL) images of representative zircons for the Neoarchean TTG and potassic granitoids in the Xingcheng regions. The solid and dashed circles on the CL images are the spots of in-situ zircon U-Pb dating and Hf isotope analyses, respectively. Also shown are the $^{207}Pb/^{206}Pb$ ages and $\varepsilon_{Hf}(t)$ values of zircons. The scale bar is 100 μm.

Fig 4 U-Pb concordia diagrams for the Neoarchean TTG and potassic granitoids in the Xingcheng region.

Fig 5 (a) (Na_2O+K_2O)-SiO_2 diagram; (b) Normative An-Ab-Or triangle diagram (Barker, 1979); (c) A/NK-A/CNK diagram; (d) Na_2O-K_2O diagram for the Neoarchean TTG and potassic granitoids in the Xingcheng region. Grey fields are the fields of experimental metabasalt melts at 1-4 GPa, which are constructed using data from Sen & Dunn (1994), Rapp & Watson (1995), Rapp *et al*. (1999, 2002, 2003), Skjerlie & Patiño Douce (2002) and references therein.

Fig 6 Harker diagrams for the Neoarchean TTG and potassic granitoids in the Xingcheng region. (a) K_2O-SiO_2; (b) P_2O_5-SiO_2; (c) TiO_2-SiO_2; (d) MgO-SiO_2; (e) Y-SiO_2; (f) Sr-SiO_2. Grey fields are the field of experimental metabasalt melts at 1-4 GPa and data sources are the same in Fig 5. The fields of slab-derived adakites and lower crust-derived adakitic rocks in Fig 6d are after Wang *et al*. (2006). The dividing line between high-Sr and low-Sr series is from Moyen *et al*. (2007). Legends are the same as those in Fig 5.

Fig 7 Chondrite-normalized REE patterns for the Neoarchean TTG and potassic granitoids in the Xingcheng region. The values of chondrite are from Sun & McDonough (1989).

Fig 8 Primitive mantle (PM)-normalized trace element diagrams for the Neoarchean TTG and potassic granitoids in the Xingcheng region. The values of PM are from Sun & McDonough (1989).

Fig 9 $\varepsilon_{Nd}(t)$-t diagram for the Neoarchean TTG and potassic granitoids in the Xingcheng region. Note that the MMEs and their host TTGs have overlapping $\varepsilon_{Nd}(t)$ values. The $\varepsilon_{Nd}(t)$ values of the potassic granitoids are also indistinguishable with those of the TTG granitoids. Legends are the same as those in Fig 5.

Fig 10 Histograms of $\varepsilon_{Hf}(t)$ values for the zircons from the Neoarchean TTG and potassic granitoids in the Xingcheng region. Note that the $\varepsilon_{Hf}(t)$ values of zircons from the Taili gneissic granite and the Xingcheng tonalite-trondhjemite are similar. The same goes for the Juhuadao granodiorite and the hosted MME and their $\varepsilon_{Hf}(t)$ values are slightly higher than those of the the Taili gneissic granite and the Xingcheng tonalite-trondhjemite. The $\varepsilon_{Hf}(t)$ values of zircons from the Xingcheng potassic granites are similar with those of the Huludao potassic granites.

Fig 11 Comparison of Hf isotopes of zircons from the Neoarchean TTG and potassic granitoids in the Xingcheng region with those of zircons from the Caozhuang complex and the

Mesoarchean TTGs in Eastern Shandong and Anshan, whose zircon Hf isotope data are from Wu *et al*. (2005a, 2014), Wan *et al*. (2007), Liu *et al*. (2013a, 2013b), Wang *et al*. (2014b), Xie *et al*. (2014). Note that almost all the data fall between the evolution lines of the depleted mantle and the chondrite uniform reservoir. The Paleo- to Eoarchean crustal materials were not involved in the generation of the Neoarchean TTG and potassic granitoids as the Paleo- to Eoarchean zircons and Mesoarchean granitoids derived from Paleo- to Eoarchean crustal materials exhibit a different evolution trend. The Mesoarchean TTGs in Eastern Shandong were derived from juvenile mafic sources, and the Neoarchean granitoids in the Xingcheng region may be derived from these Mesoarchean TTGs and their juvenile mafic sources.

Fig 12 Co-variation diagrams of (a) Chondrite-normalized $(La/Yb)_N$-$(Yb)_N$; (b) Sr/Y-Y; (c) $Mg^{\#}$-SiO_2 and (d) Dy/Yb- SiO_2 for the Neoarchean TTG and potassic granitoids in the Xingcheng region. In Fig 12a, batch melting curves of an EMORB-like source (Sun & McDonough, 1989) were constructed using partition coefficients of Bédard (2006). In Fig 12c, crustal AFC process of mantle derived mafic melts is from Yang et al. (2008). Data sources of Fig 12c are the same as those in Figs 5 and 6d. Legends are the same as those in Fig 5.

Fig 13 (a) ΔSr-ΔRb; (b) ΔSr-ΔTh; (c) ΔY-ΔRb and (d) ΔNb-K_2O/Na_2O diagrams for the Neoarchean granitoids in the Xingcheng region. For X as any give element, the ΔX parameter (ΔX = X – (a SiO_2 + b); constants a and b are empirically estimated by Moyen *et al*., 2010) expresses the distance between the analyzed value and a reference line in an X-SiO_2 (Harker) diagram, which removes the contribution of SiO_2-related evolution. The vertical axes of these

diagrams were built using pressure/depth-controlled elements and the horizontal axes were built using source enrichment-controlled elements/ratios. These diagrams can simultaneously reveal information about both the source composition/enrichment and the depth/pressure of melting. In these diagrams, the vectors showing the trends of these parameters towards higher pressures and richer sources are from Moyen *et al*. (2010). Note that two Huludao potassic granites with extremely high K_2O/Na_2O ratios were omitted in (d). Legends are the same as those in Fig 5.

Fig 14 Primitive mantle (PM)-normalized trace element diagram for the average compositions of TTG granitoids and potassic granites and calculated compositions of Archean upper continental crust in the Xingcheng (This study) and Qinhuangdao (Yang et al., 2008) regions assuming TTG granitoids/potassic granites = 9:1. The composition of present-day upper continental crust (Rudnick & Gao, 2003) is also plotted for comparison. The values of PM are from Sun & McDonough (1989).

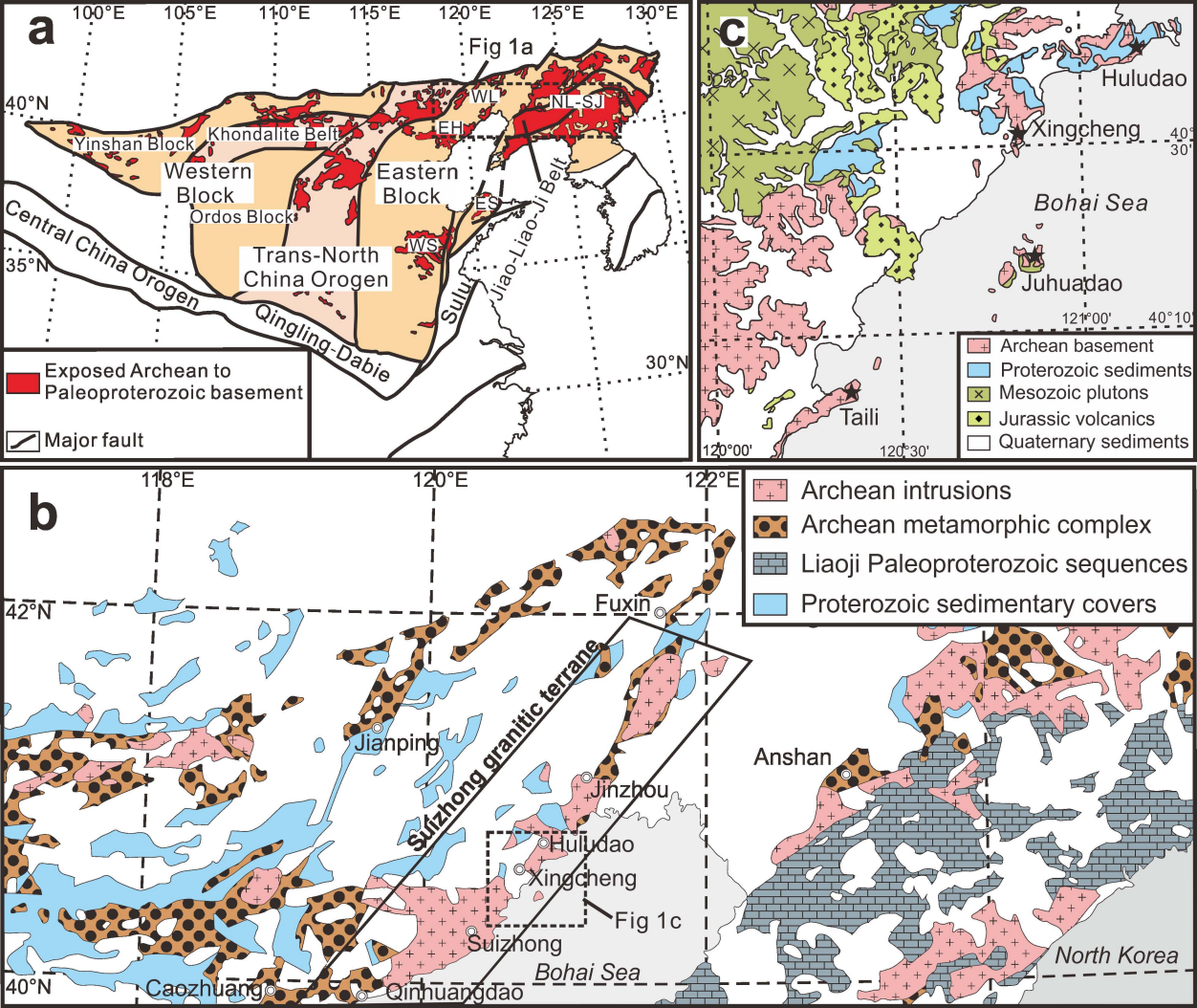
a
100°E
105°E
110°E
115°E
120°E
125°E
130°E
40°N
35°N
30°N
Fig 1a
WL
NL-SJ
EH
ES
WS
Yinshan Block
Khondalite Belt
Western Block
Eastern Block
Ordos Block
Trans-North China Orogen
Central China Orogen
Qingling-Dabie
Sulu
Jiao-Liao-Ji Belt
Exposed Archean to Paleoproterozoic basement
Major fault
c
Huludao
Xingcheng
40°30'
Bohai Sea
Juhuadao
121°00'
40°10'
Taili
120°00'
120°30'
Archean basement
Proterozoic sediments
Mesozoic plutons
Jurassic volcanics
Quaternary sediments
b
118°E
120°E
122°E
42°N
40°N
Archean intrusions
Archean metamorphic complex
Liaoji Paleoproterozoic sequences
Proterozoic sedimentary covers
Fuxin
Jianping
Suizhong granitic terrane
Jinzhou
Anshan
Huludao
Xingcheng
Fig 1c
Suizhong
Bohai Sea
North Korea
Caozhuang
Qinhuangdao

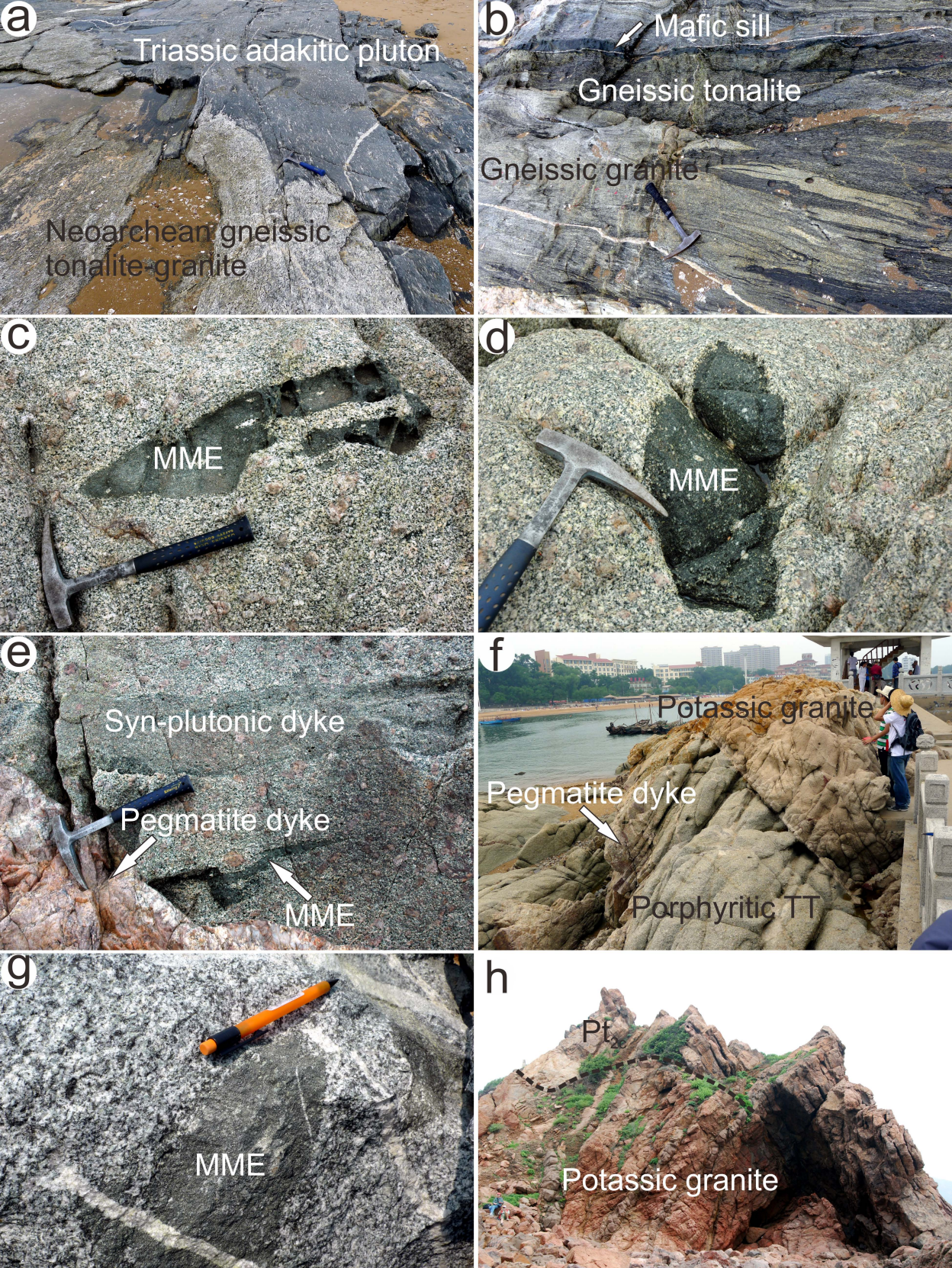
a
Triassic adakitic pluton
Neoarchean gneissic tonalite-granite
b
Mafic sill
Gneissic tonalite
Gneissic granite
c
MME
d
MME
e
Syn-plutonic dyke
Pegmatite dyke
MME
f
Potassic granite
Pegmatite dyke
Porphyritic TT
g
MME
h
Pt_2c
Potassic granite

10TL13
1.1

2541 ± 18 Ma

10XC02
2.1

2452 ± 20 Ma

11XC03
8.1

2485 ± 30 Ma

12XC22
7.1

2577 ± 17 Ma

12XC28
4.1

2541 ± 21 Ma

12XC15
14.1

2547 ± 17 Ma

10XC05
8.1

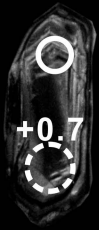

2460 ± 15 Ma

10XC08
3.1

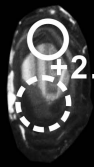

2494 ± 18 Ma

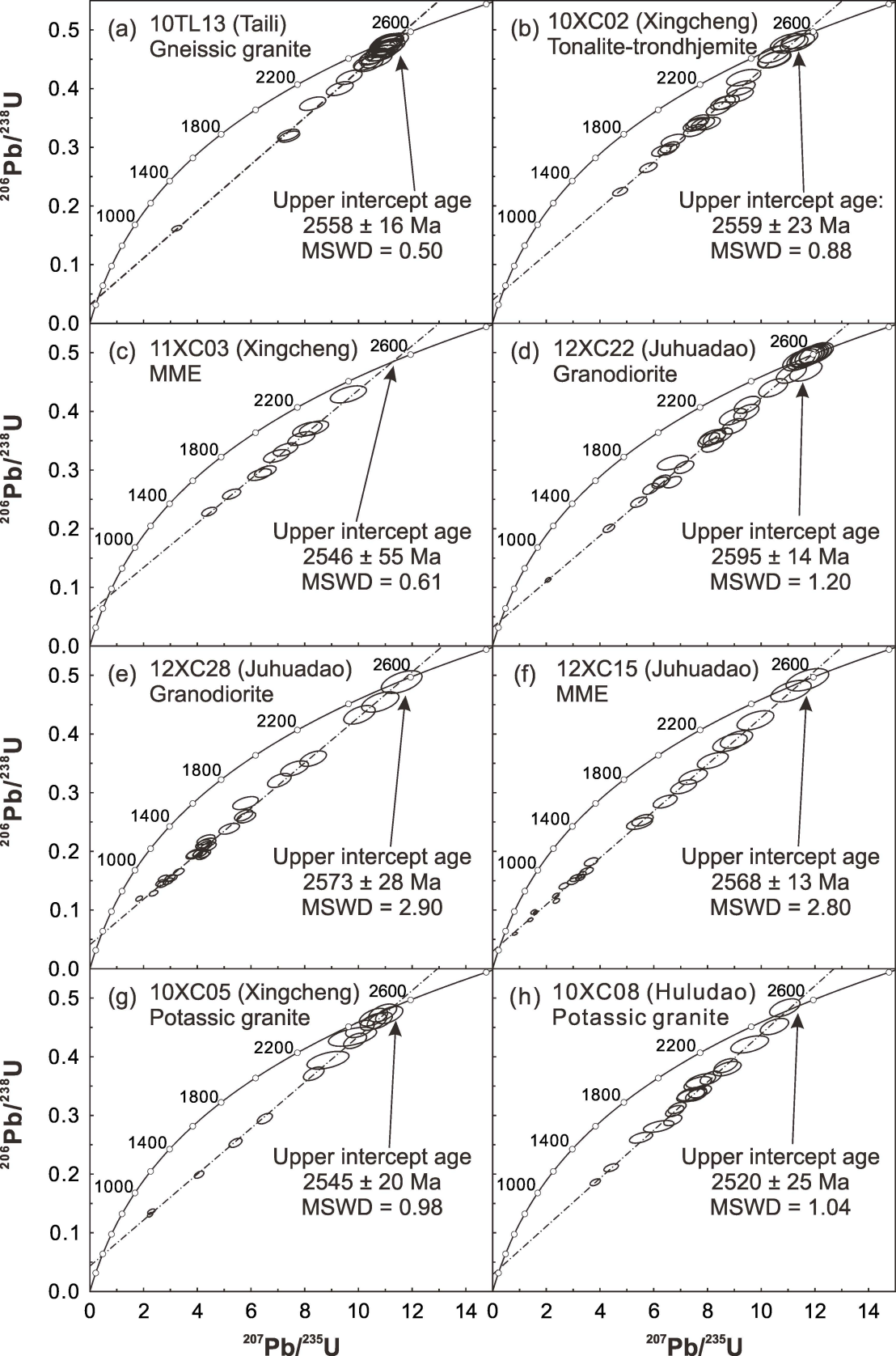
(a) 10TL13 (Taili)
Gneissic granite
Upper intercept age
2558 ± 16 Ma
MSWD = 0.50
(b) 10XC02 (Xingcheng)
Tonalite-trondhjemite
Upper intercept age:
2559 ± 23 Ma
MSWD = 0.88
(c) 11XC03 (Xingcheng)
MME
Upper intercept age
2546 ± 55 Ma
MSWD = 0.61
(d) 12XC22 (Juhuadao)
Granodiorite
Upper intercept age
2595 ± 14 Ma
MSWD = 1.20
(e) 12XC28 (Juhuadao)
Granodiorite
Upper intercept age
2573 ± 28 Ma
MSWD = 2.90
(f) 12XC15 (Juhuadao)
MME
Upper intercept age
2568 ± 13 Ma
MSWD = 2.80
(g) 10XC05 (Xingcheng)
Potassic granite
Upper intercept age
2545 ± 20 Ma
MSWD = 0.98
(h) 10XC08 (Huludao)
Potassic granite
Upper intercept age
2520 ± 25 Ma
MSWD = 1.04
1000
1400
1800
2200
2600
$^{206}Pb/^{238}U$
$^{207}Pb/^{235}U$

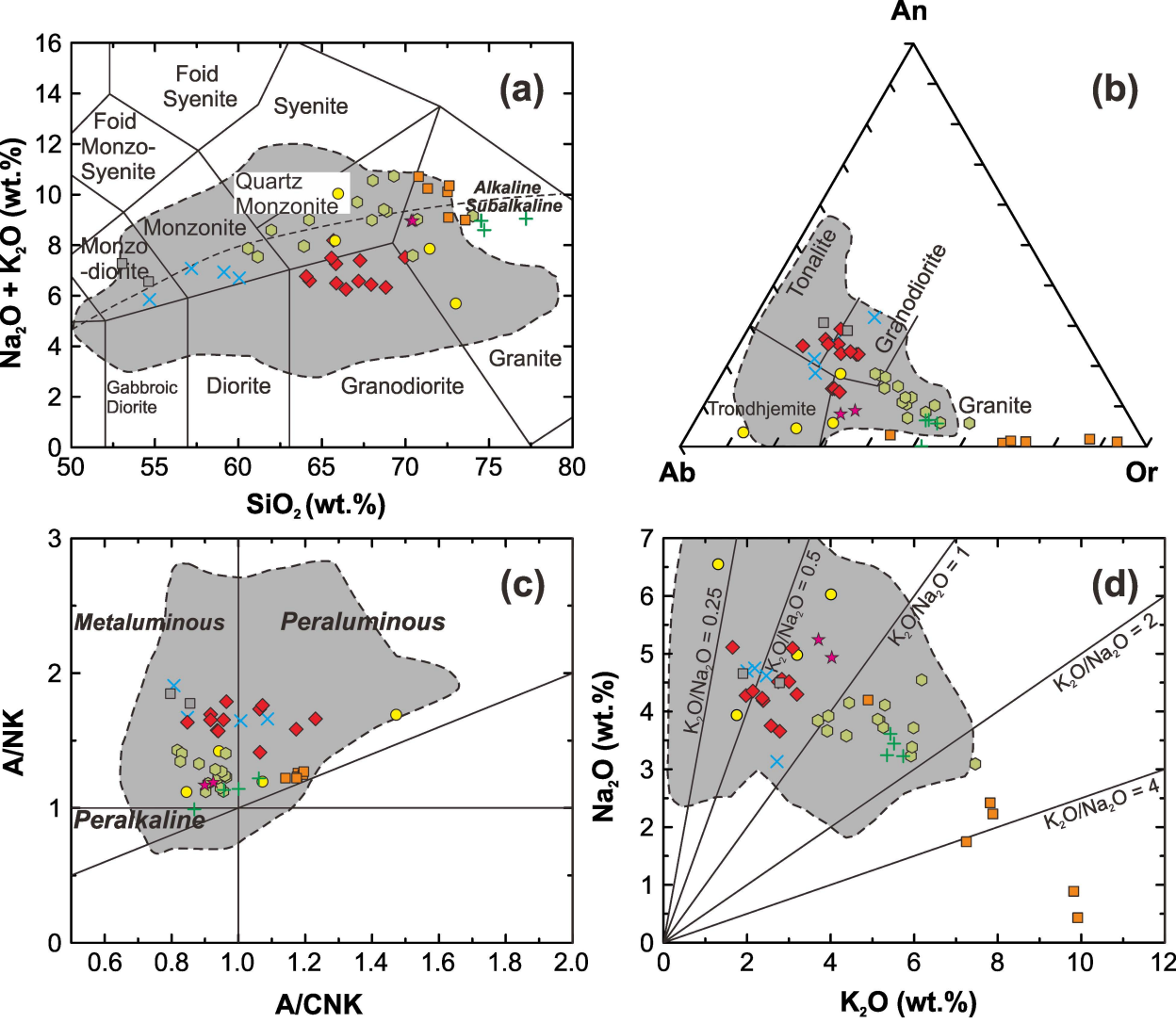
(a)
Foid Syenite
Syenite
Foid Monzo-Syenite
Quartz Monzonite
Alkaline
Subalkaline
Monzonite
Monzo-diorite
Granite
Gabbroic Diorite
Diorite
Granodiorite
Na2O + K2O (wt.%)
SiO2 (wt.%)
(b)
An
Tonalite
Granodiorite
Trondhjemite
Granite
Ab
Or
(c)
Metaluminous
Peraluminous
Peralkaline
A/NK
A/CNK
(d)
K2O/Na2O = 0.25
K2O/Na2O = 0.5
K2O/Na2O = 1
K2O/Na2O = 2
K2O/Na2O = 4
Na2O (wt.%)
K2O (wt.%)
Gneissic granite-Taili
Gneissic tonalite-Taili
Tonalite-trondhjemite-Xingcheng
Granodiorite-Juhuadao
MME-Xingcheng
MME-Juhuadao
Potassic granite-Xingcheng
Potassic granite-Huludao

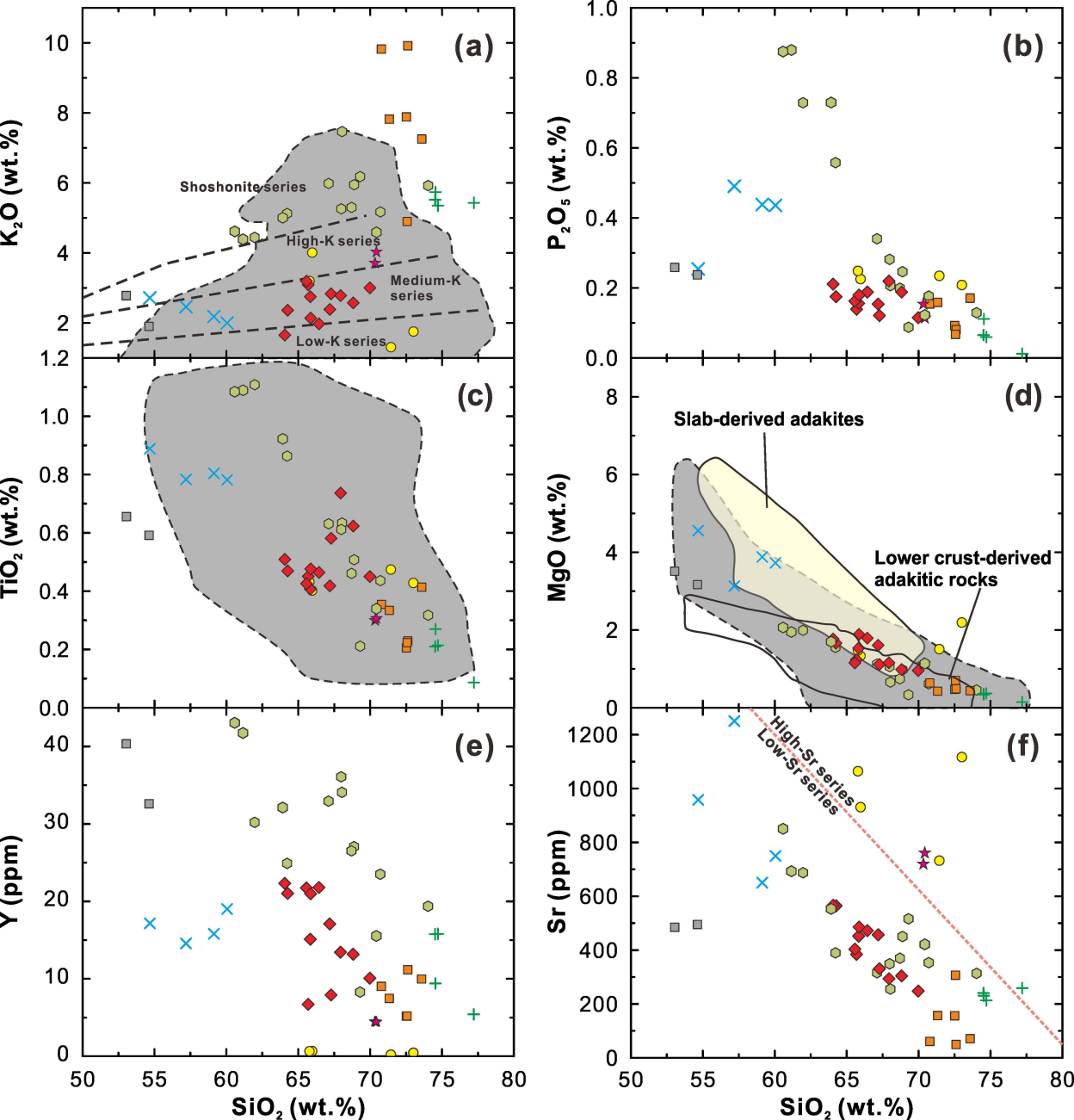
(a)
(b)
(c)
(d)
(e)
(f)
K_2O (wt.%)
P_2O_5 (wt.%)
TiO_2 (wt.%)
MgO (wt.%)
Y (ppm)
Sr (ppm)
SiO_2 (wt.%)
SiO_2 (wt.%)
Shoshonite series
High-K series
Medium-K series
Low-K series
Slab-derived adakites
Lower crust-derived adakitic rocks
High-Sr series
Low-Sr series

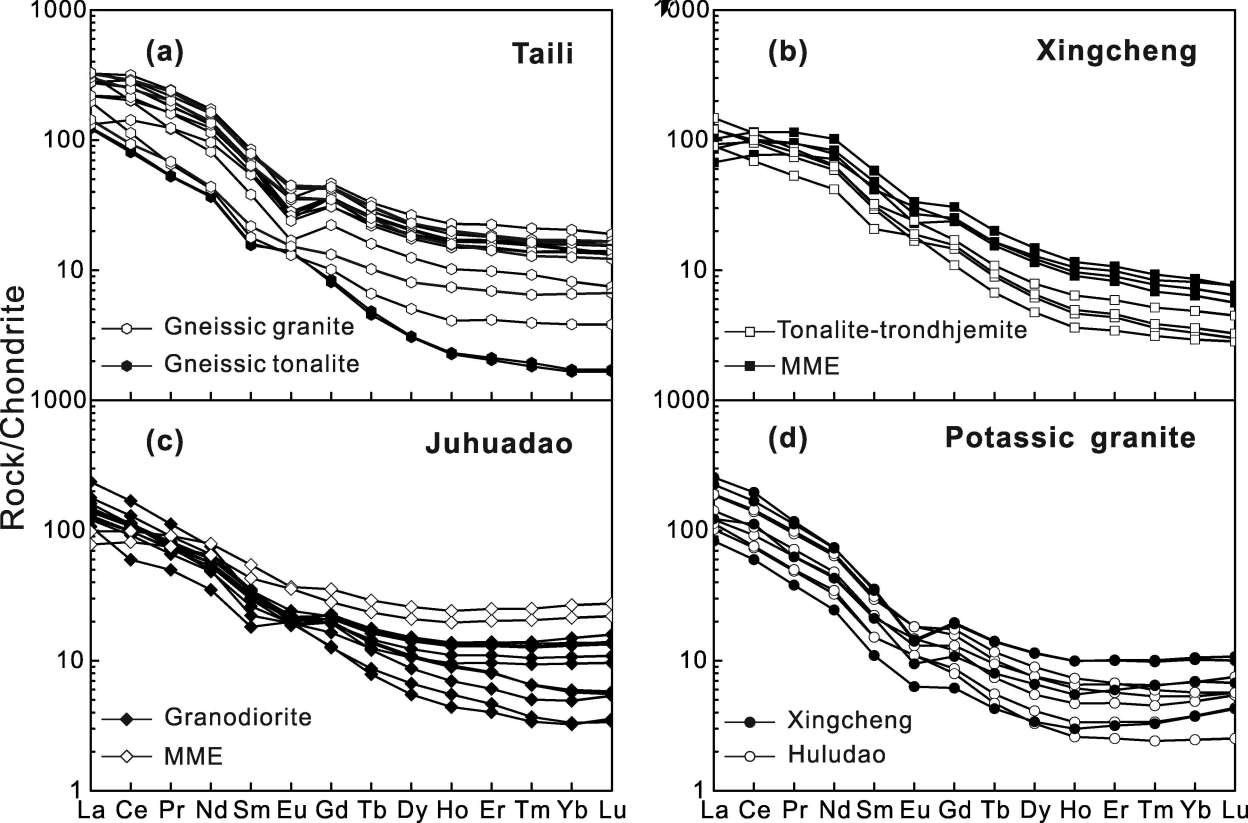
(a)
Taili
Gneissic granite
Gneissic tonalite
(b)
Xingcheng
Tonalite-trondhjemite
MME
(c)
Juhuadao
Granodiorite
MME
(d)
Potassic granite
Xingcheng
Huludao
Rock/Chondrite
1000
100
10
1
La Ce Pr Nd Sm Eu Gd Tb Dy Ho Er Tm Yb Lu

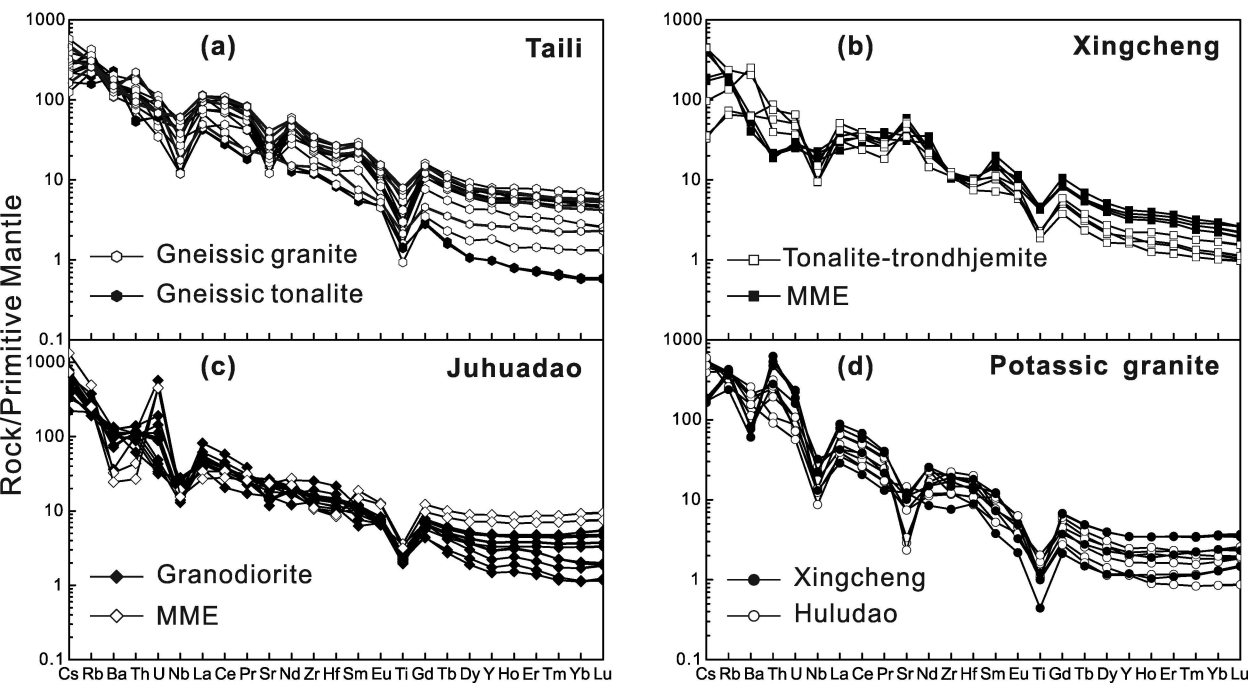
(a)
Taili
Gneissic granite
Gneissic tonalite
(b)
Xingcheng
Tonalite-trondhjemite
MME
(c)
Juhuadao
Granodiorite
MME
(d)
Potassic granite
Xingcheng
Huludao
Rock/Primitive Mantle
1000
100
10
1
0.1
Cs Rb Ba Th U Nb La Ce Pr Sr Nd Zr Hf Sm Eu Ti Gd Tb Dy Y Ho Er Tm Yb Lu

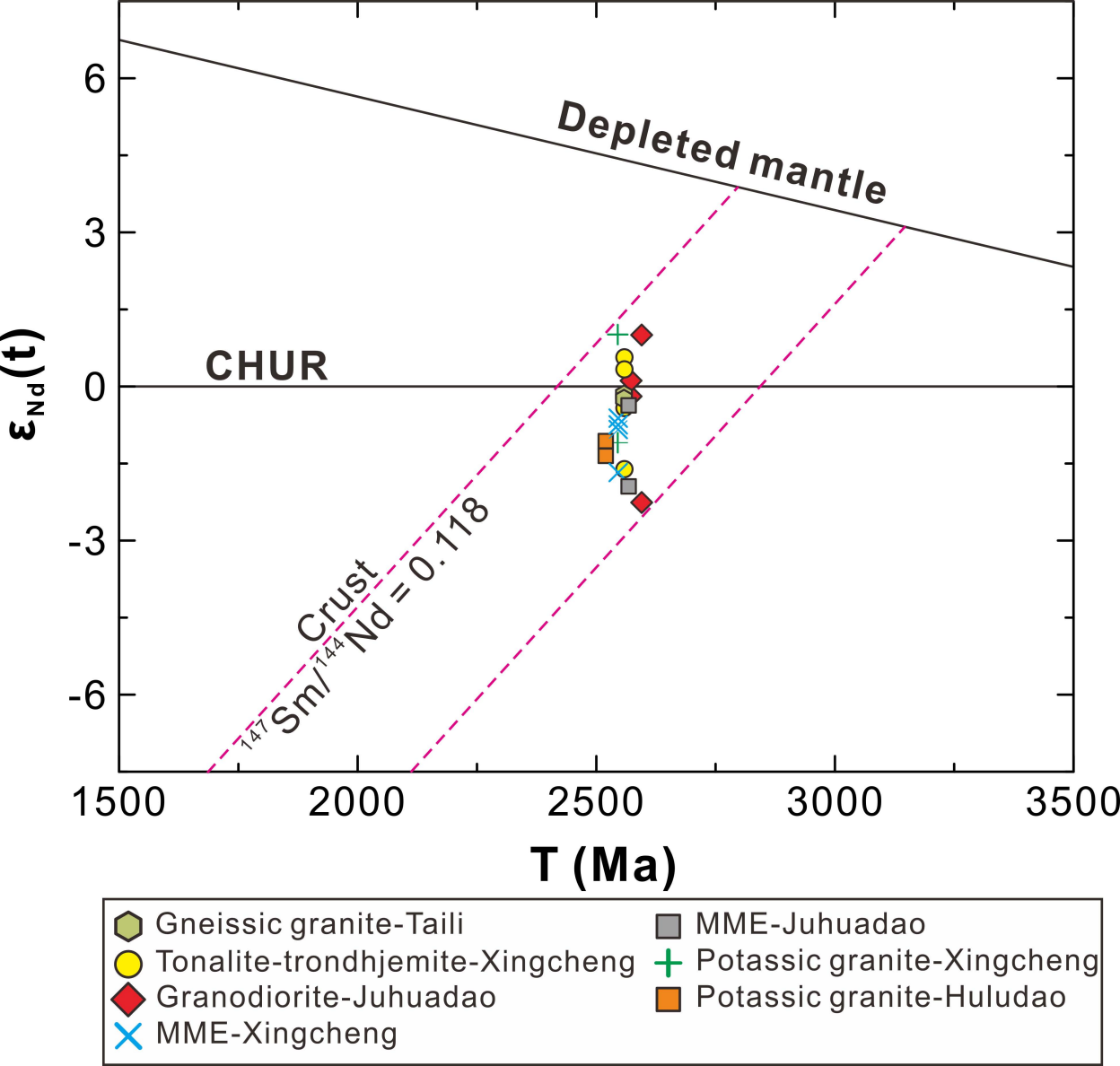
Depleted mantle
CHUR
Crust
$^{147}Sm/^{144}Nd = 0.118$
$\varepsilon_{Nd}(t)$
T (Ma)
6
3
0
-3
-6
1500
2000
2500
3000
3500
Gneissic granite-Taili
Tonalite-trondhjemite-Xingcheng
Granodiorite-Juhuadao
MME-Xingcheng
MME-Juhuadao
Potassic granite-Xingcheng
Potassic granite-Huludao

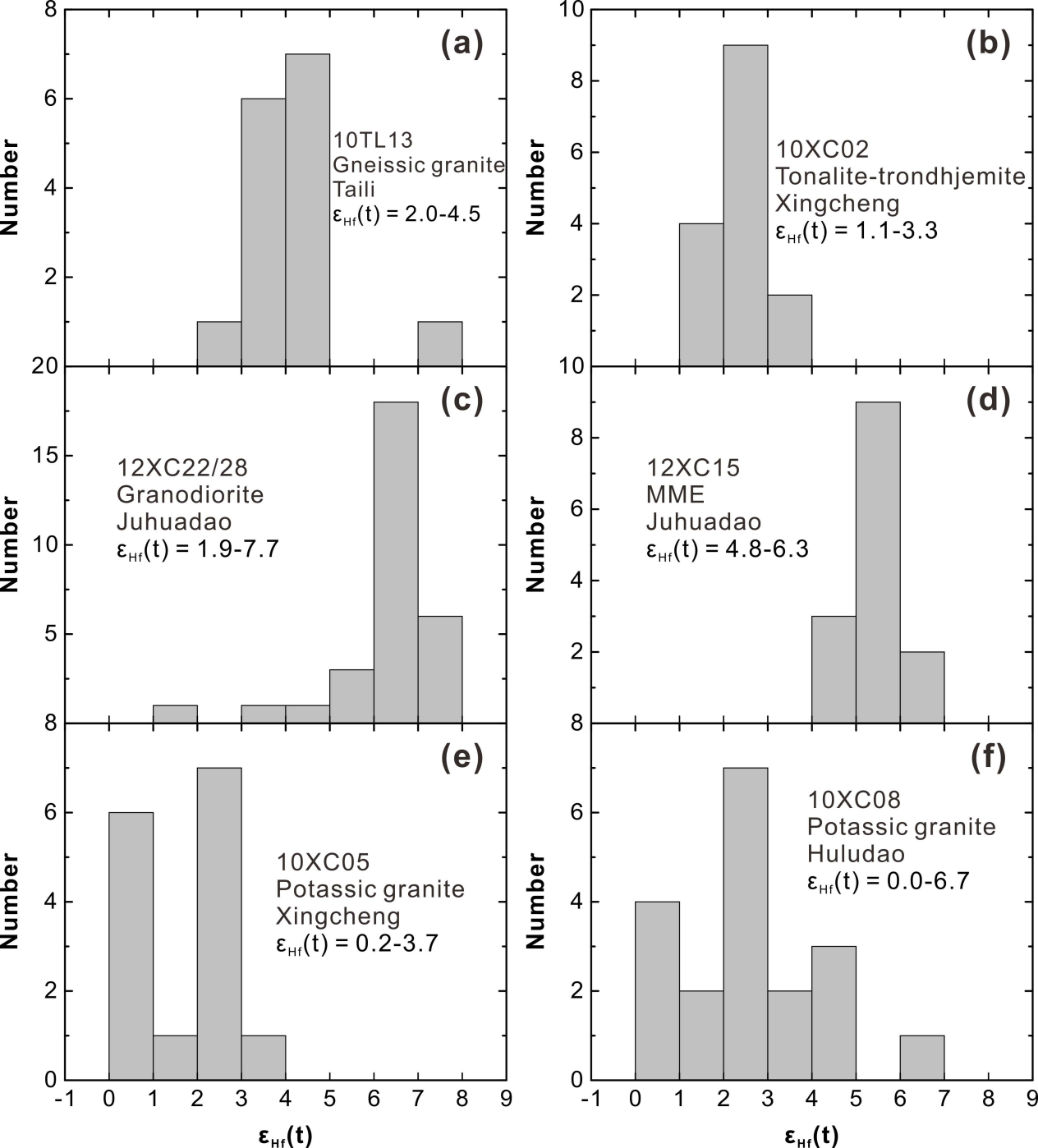
(a)
10TL13
Gneissic granite
Taili
εHf(t) = 2.0-4.5
(b)
10XC02
Tonalite-trondhjemite
Xingcheng
εHf(t) = 1.1-3.3
(c)
12XC22/28
Granodiorite
Juhuadao
εHf(t) = 1.9-7.7
(d)
12XC15
MME
Juhuadao
εHf(t) = 4.8-6.3
(e)
10XC05
Potassic granite
Xingcheng
εHf(t) = 0.2-3.7
(f)
10XC08
Potassic granite
Huludao
εHf(t) = 0.0-6.7
Number
εHf(t)

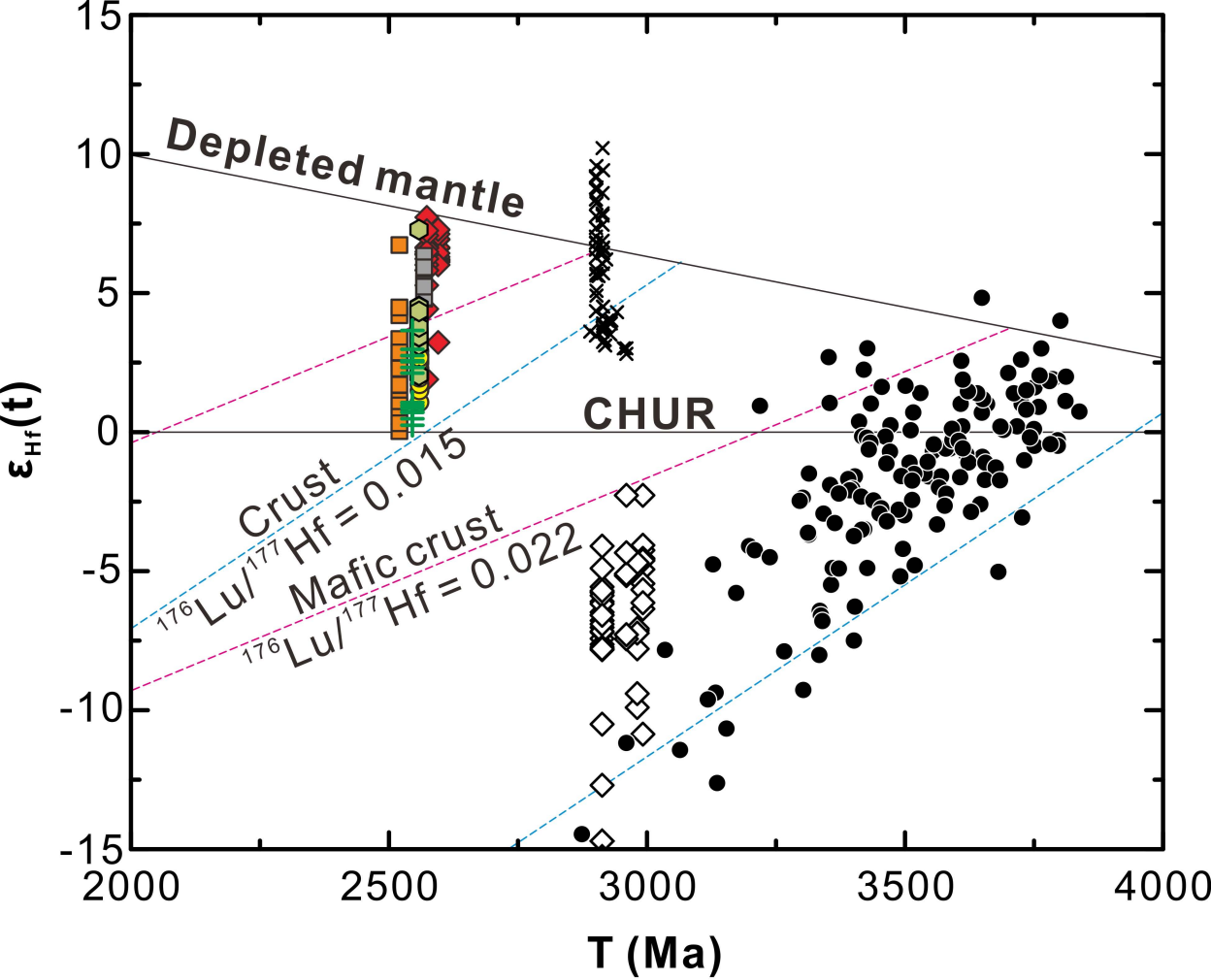
Depleted mantle
CHUR
Crust
$^{176}Lu/^{177}Hf = 0.015$
Mafic crust
$^{176}Lu/^{177}Hf = 0.022$
$\varepsilon_{Hf}(t)$
T (Ma)
15
10
5
0
-5
-10
-15
2000
2500
3000
3500
4000
Gneissic granite-Taili
Tonalite-trondhjemite-Xingcheng
Granodiorite-Juhuadao
MME-Juhuadao
Mesoarchean TTG-Eastern Shandong
Potassic granite-Xingcheng
Potassic granite-Huludao
Caozhuang complex
Tiejiashan granite-Anshan

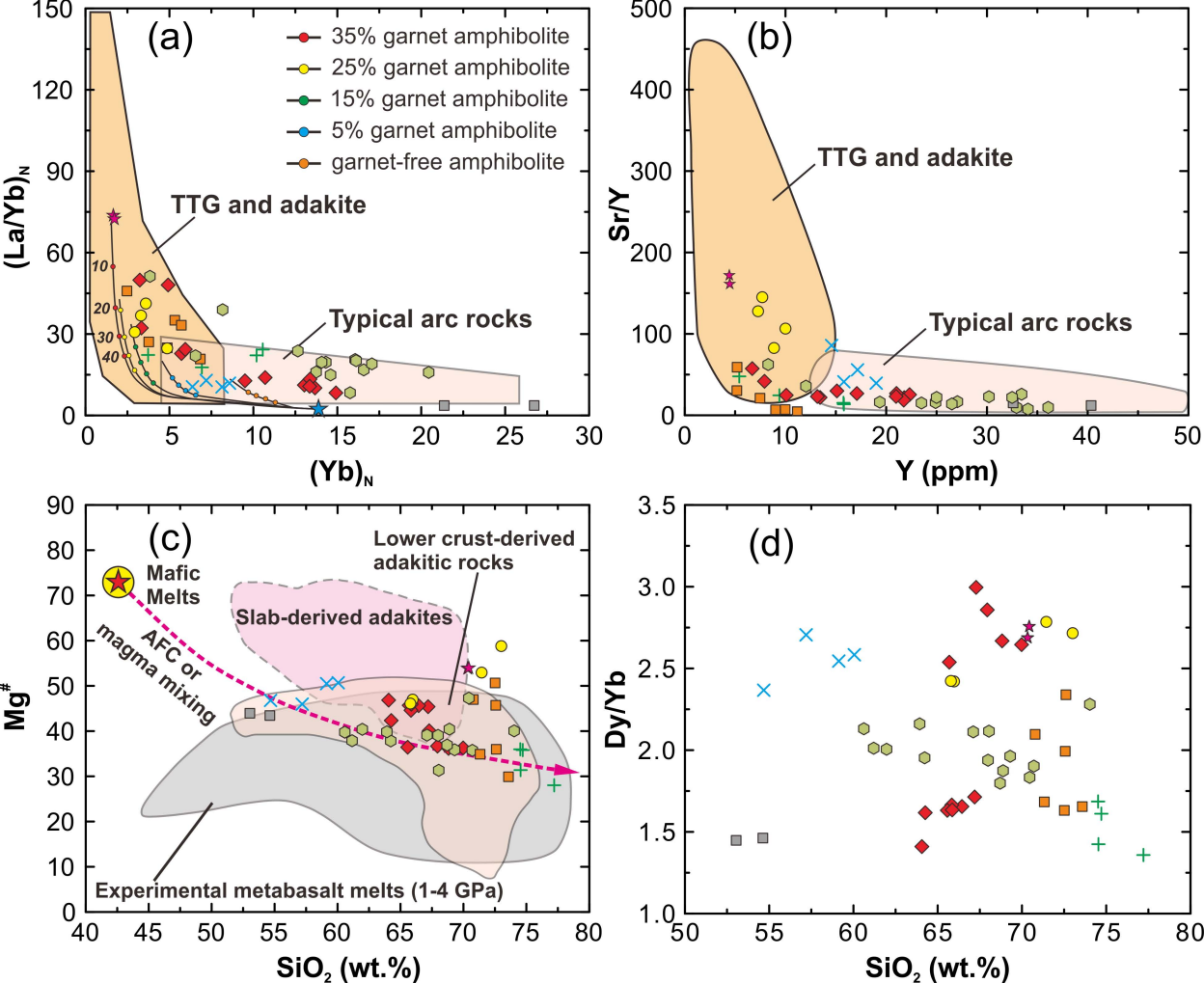
(a)
35% garnet amphibolite
25% garnet amphibolite
15% garnet amphibolite
5% garnet amphibolite
garnet-free amphibolite
TTG and adakite
Typical arc rocks
10
20
30
40
(La/Yb)N
(Yb)N
(b)
TTG and adakite
Typical arc rocks
Sr/Y
Y (ppm)
(c)
Mafic Melts
AFC or magma mixing
Lower crust-derived adakitic rocks
Slab-derived adakites
Experimental metabasalt melts (1-4 GPa)
Mg#
SiO2 (wt.%)
(d)
Dy/Yb
SiO2 (wt.%)

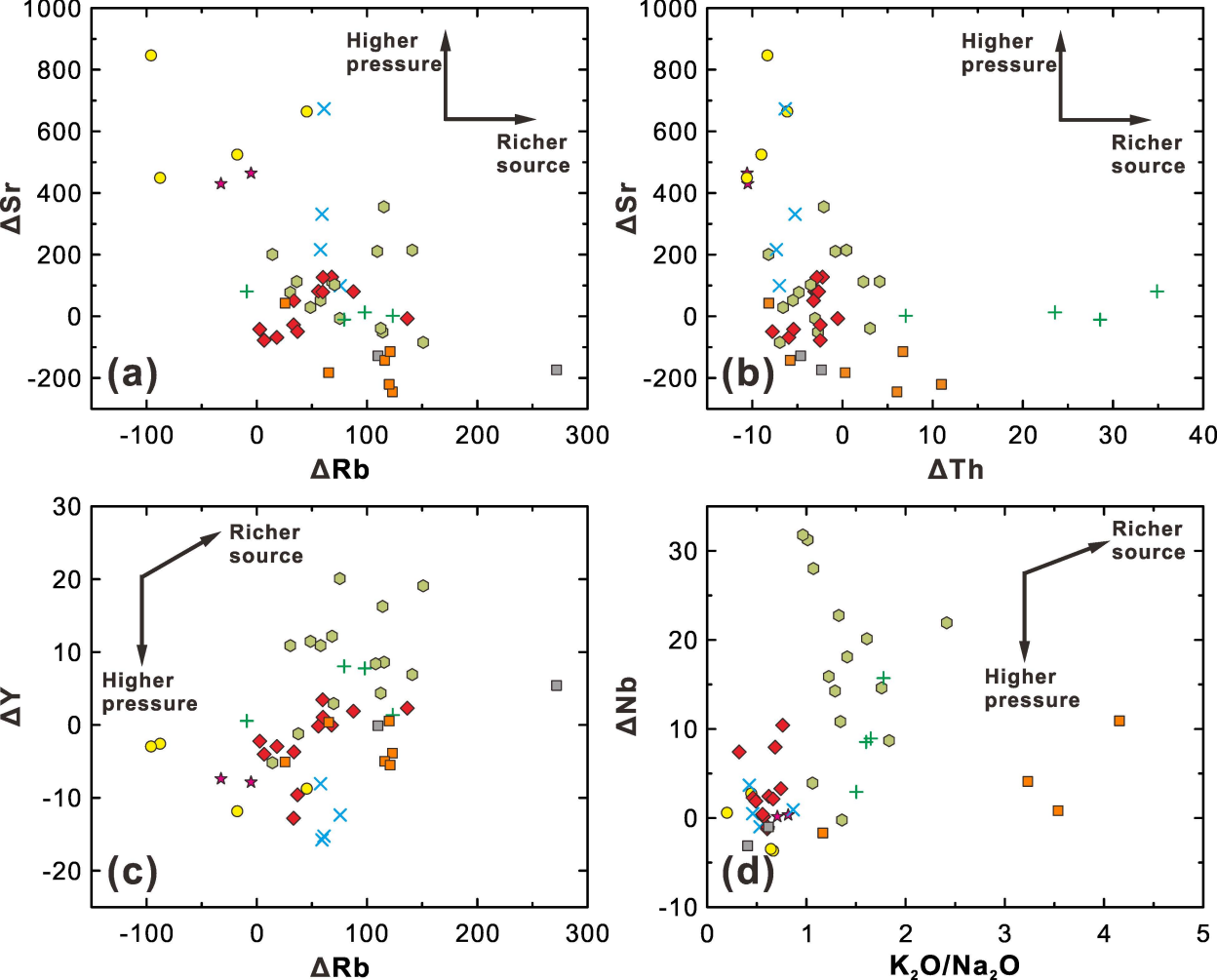
(a)
Higher pressure
Richer source
ΔSr
ΔRb
(b)
Higher pressure
Richer source
ΔSr
ΔTh
(c)
Richer source
Higher pressure
ΔY
ΔRb
(d)
Richer source
Higher pressure
ΔNb
K2O/Na2O

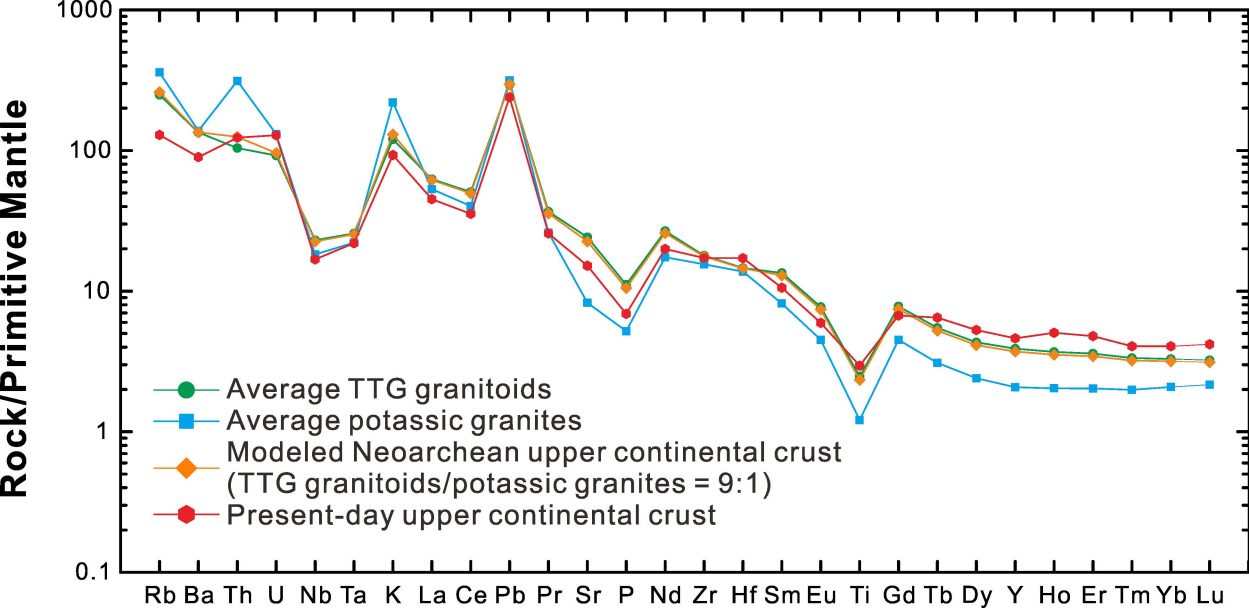
Rock/Primitive Mantle
1000
100
10
1
0.1
Average TTG granitoids
Average potassic granites
Modeled Neoarchean upper continental crust
(TTG granitoids/potassic granites = 9:1)
Present-day upper continental crust
Rb Ba Th U Nb Ta K La Ce Pb Pr Sr P Nd Zr Hf Sm Eu Ti Gd Tb Dy Y Ho Er Tm Yb Lu